Published in final edited form as:
Nature. 2020 March 01; 579(7799): 433–437. doi:10.1038/s41586-020-2076-4.

A pathway coordinated by DELE1 relays mitochondrial stress to the cytosol

Evelyn Fessler, **Eva-Maria Eckl**, **Sabine Schmitt**, **Igor Alves Mancilla**, **Matthias F. Meyer-Bender**, **Monika Hanf**, **Julia Philippou-Massier**, **Stefan Krebs**, **Hans Zischka**, **Lucas T. Jae**

[1]Gene Center and Department of Biochemistry, Ludwig-Maximilians-Universität München, Munich, Germany

[2]Institute of Toxicology and Environmental Hygiene, School of Medicine, Technical University Munich, Munich, Germany

[3]Institute of Molecular Toxicology and Pharmacology, Helmholtz Center Munich, German Research Center for Environmental Health, Neuherberg, Germany

Abstract

Mitochondrial fidelity is tightly linked to overall cellular homeostasis and is compromised in ageing and various pathologies[1,2,3]. Mitochondrial malfunction needs to be relayed to the cytosol, where an integrated stress response is triggered by the phosphorylation of eukaryotic translation initiation factor 2α (eIF2α) in mammalian cells[4,5]. eIF2α phosphorylation is mediated by the four eIF2α kinases GCN2, HRI, PERK and PKR, which are activated by diverse types of cellular stress[6]. However, the machinery that communicates mitochondrial perturbation to the cytosol to trigger the integrated stress response remains unknown[1,2,7]. Here we combine genome engineering and haploid genetics to unbiasedly identify genes that affect the induction of C/EBP homologous protein (CHOP), a key factor in the integrated stress response. We show that the mitochondrial protease OMA1 and the poorly characterized protein DELE1, together with HRI, constitute the missing pathway that is triggered by mitochondrial stress. Mechanistically, stress-induced activation of OMA1 causes DELE1 to be cleaved into a short form that accumulates in the cytosol, where it binds to and activates HRI via its C-terminal portion. Obstruction of this pathway can be beneficial or adverse depending on the type of mitochondrial perturbation. In addition to the core pathway components, our comparative genetic screening strategy identifies a suite of additional regulators. Together, these findings could be used to inform future strategies to modulate the cellular response to mitochondrial dysfunction in the context of human disease.

Despite their partial autonomy, mitochondria do not encode stress-response genes[1]. Instead, CHOP—a core component of the integrated stress response (ISR)—is among the most

Correspondence to: Lucas T. Jae.

Corresponding author: Correspondence to Lucas T. Jae.

Contributions

E.F. and L.T.J. conceived the study; E.F., E.-M.E. and L.T.J. performed experiments and analysed data; S.S. performed mitochondrial isolations and subsequent in vitro stimulations; I.A.M. generated knockout cell lines; M.F.M.-B. performed bioinformatics analyses; J.P.-M. generated and analysed RNA-seq libraries; S.K. performed deep sequencing; M.H. constructed plasmids; H.Z. and L.T.J. supervised experiments; E.F. and L.T.J. wrote the manuscript with input from all authors.

Europe PMC Funders Author Manuscripts

strongly induced factors in cells that are challenged by inhibition of either the mitochondrial matrix chaperone TRAP1 (by gamitrinib-triphenylphosphonium (GTPP)) or the mitochondrial protease LON (by CDDO)[7]. Because of their roles in protein folding and protein removal, respectively, inhibition of TRAP1 or LON causes the misfolding of proteins in the mitochondrial matrix. CHOP is a transcription factor that is able to tune the cellular response to different cues through initiation of apoptotic and non-apoptotic programs[8]. *DDIT3*, the gene that encodes CHOP, is itself a target of the transcription factor ATF4—another key component of the ISR[1,7]. In addition, the synthesis of CHOP underlies regulation at the level of translation through an upstream open reading frame (uORF) that inhibits the generation of CHOP under basal conditions. Although phosphorylation of eIF2α at Ser51 reduces protein synthesis globally, it stimulates translation of CHOP, thus overriding the inhibitory effect of the upstream open reading frame[2,8].

Genome-wide perturbation screens

Whereas treating HAP1 cells with tunicamycin, CDDO or the mitochondrial ionophore CCCP (carbonyl cyanide m-chlorophenyl hydrazone) did not trigger profound changes in the abundance of the heat-shock protein HSPD1, all of these stressors led to a strong induction of CHOP (Extended Data Fig. 1a, b). To accurately capture the production of CHOP protein, we generated HAP1 cells that endogenously express CHOP as a fusion protein with mNeon from the *DDIT3* locus (CHOP^{Neon}). A clonal population of the engineered cells responded to a challenge with CCCP, CDDO or tunicamycin by induction of CHOP^{Neon} (Extended Data Fig. 1c, d). We then subjected haploid CHOP^{Neon} cells to random genome mutagenesis by gene trapping, challenged them with CCCP and sequenced mutations in cell populations in which the induction of CHOP^{Neon} was diminished or enhanced[9] (Extended Data Fig. 1e). We found that mutants defective in CHOP itself or its upstream transcriptional inducer ATF4 were strongly enriched among cells that poorly induced CHOP^{Neon}, together with a wealth of other regulators (Fig. 1a, Supplementary Table 1). To distinguish general regulators of CHOP from context-specific factors, we performed two additional orthogonal genome-wide screens using tunicamycin or CDDO (Fig. 1b, Extended Data Fig. 1f, Supplementary Tables 2, 3). In line with its inhibitory effect on *N*-glycosylation[10], treatment with tunicamycin highlighted numerous genes that are associated with the maturation and quality control of endoplasmicreticulum proteins, as well as the canonical eIF2α kinase activated after endoplasmic-reticulum stress: PERK[1,2]. By contrast, the effects of CDDO on CHOP were not blunted by the deficiency in any individual eIF2α kinase[7] (Extended Data Fig. 1g), possibly owing to the limited specificity of related compounds[11]. The comparative interrogation of CHOP regulators in relation to three distinct types of cellular stress allowed us to differentiate global regulators of CHOP biology (Extended Data Fig. 1h–m) from those that selectively operate in the context of CCCP-induced mitochondrial depolarization (Extended Data Figs. 2–4). In particular, stringent filtering for genes that prominently scored with CCCP, but not with tunicamycin or CDDO, highlighted the transcriptional regulators TAF4 and GABPB1, the glycolysis factors SLC2A1 and TPI1 and the RNA-binding proteins RBM27 and CLUH. The signature also contained the mitochondrial proteins ATP5IF1 and OMA1. Most notably, it revealed a strong requirement for HRI (encoded by *EIF2AK1*) and the little-studied protein DELE1 (Fig. 1a, Extended Data Fig. 5a, b).

Cellular dynamics of DELE1

Given the scarcity of existing knowledge on DELE1 and the unexpected involvement of HRI, we first sought to validate their requirement in a panel of cell systems that included non-transformed cells. We were able to confirm the importance of DELE1 and HRI in all cases (Extended Data Fig. 5c). Furthermore, induction of CHOP also depended on DELE1 and HRI under other types of mitochondrial stress, including oligomycin-mediated inhibition of complex V, GTPP-mediated inhibition of TRAP1 and genetic ablation of *LONP1* (Extended Data Fig. 5d–f). The failure of cells to induce CHOP after stimulation with CCCP was preceded by a defect in the phosphorylation of eIF2α in HRI- or DELE1-deficient cells, suggesting that—like HRI—DELE1 operates upstream of this event (Extended Data Fig. 5g). Notably, expression of HRI in DELE1-knockout cells was able to partially restore CHOP induction, whereas expression of DELE1 in HRI-deficient cells had no discernible effect (Fig. 2a, Extended Data Fig. 6a, b). This indicates that DELE1 requires HRI to trigger CHOP, but not vice versa, and that DELE1 therefore probably acts upstream of both eIF2α and HRI. As DELE1 is a mitochondrial protein[12] (Extended Data Fig. 6c), whereas HRI is cytoplasmic, we next wondered whether the activity of DELE1 in relation to HRI might be regulated by its localization. To test this hypothesis, we investigated whether artificially re-routing DELE1 to the cytosol would bypass the need for mitochondrial perturbation to induce CHOP. Expression of a mutant version of DELE1 that lacks the mitochondrial targeting sequence (DELE1(ΔMTS)) yielded a predominantly cytoplasmic protein that readily induced CHOP expression independently of CCCP (Fig. 2b, c, Extended Data Fig. 6d, e). This constitutively active version of DELE1 still required HRI to induce CHOP, underscoring the probable role of DELE1 as an activator of HRI.

On the basis of these findings, we asked whether the activity of wild-type DELE1 might be regulated through a similar mechanism. Whereas DELE1 localized to the mitochondria in unperturbed cells, it could be detected in the cytosol after treatment with CCCP (Fig. 2d). We did not observe this behaviour for MFN2, a mitochondrial protein that is affected by CCCP on similar timescales[13]. The redistribution of DELE1 to the cytosol was rapid and still occurred when de novo protein synthesis was blocked, suggesting that it is mediated by a post-translational event (Extended Data Fig. 6f). Time-resolved immunoblotting of exogenously expressed or endogenously tagged DELE1 after treatment with CCCP revealed a reduction in molecular weight that coincided with its cytosolic accumulation and was preserved in the absence of HRI (Fig. 2e, Extended Data Fig. 6g, h). This processing could also be observed across different types of mitochondrial stress and different cell systems—including primary cells—reinforcing the notion that the size reduction and the localization of DELE1 are associated with its cellular function (Fig. 2f, Extended Data Fig. 6i–o).

OMA1-mediated processing

Our comparative genetic screens also identified a role for the inner mitochondrial membrane metallopeptidase OMA1 in the dataset in which CHOP expression was triggered by CCCP; this role for OMA1 was not shared with the tunicamycin and CDDO datasets (Fig. 1, Extended Data Fig. 7a). Although OMA1 is mostly dormant in unstressed cells, its activity can be induced by the perturbation of mitochondrial homeostasis, leading to processing of

the inner mitochondrial membrane fusion factor OPA1 and culminating in its own destruction[14](Fig. 2f). As the precise triggers and substrate specificity of OMA1 are incompletely understood, we wondered whether DELE1 might be a target of stress-activated OMA1. Whereas wild-type cells readily generated the short version of DELE1 (S-DELE1) after CCCP treatment, this processing was virtually blocked in OMA1-knockout cells or cells that express the catalytically dead variant OMA1(E328Q)[15], and it was reduced by pharmacological inhibition of metallopeptidases but not that of other classes of proteases[14](Fig. 2g, Extended Data Fig. 7b–e). This prompted us to investigate whether OMA1-mediated cleavage of DELE1 would have an effect on its subcellular redistribution. We observed that cytosolic localization of DELE1 after exposure to CCCP was diminished in OMA1-knockout cells and cells that express catalytically dead OMA1, but could be restored by expression of wild-type OMA1 (Fig. 2h). Cleavage of wild-type DELE1 also occurred in an OMA1-dependent fashion in isolated mitochondria that were depolarized in vitro, and S-DELE1 was detectable in the mitochondrial supernatant (Extended Data Fig. 7f–k). Notably, whereas CCCP treatment led to processing of DELE1 and OPA1 on similar timescales, the cleavage and cytosolic accumulation of DELE1 occurred regardless of OPA1 status (Extended Data Fig. 8a–f).

Interaction with HRI

We next investigated how S-DELE1 might lead to activation of HRI in the cytosol. As processed DELE1 should mostly consist of tetratricopeptide repeat (TPR) domains, which mediate protein–protein interactions[16], we speculated that it might activate HRI through physical association. To test this hypothesis, we co-expressed HRI with DELE1(ΔMTS) or full-length DELE1, treated cells with CCCP and precipitated HRI-bound proteins. This showed that DELE1(ΔMTS) engaged in a constitutive interaction with HRI, whereas full-length DELE1 was only efficiently co-precipitated after being converted into S-DELE1 (Extended Data Fig. 9a). The same behaviour was observed for the endogenous proteins (Fig. 3a). Stimulation of cells with CCCP or through expression of DELE1(ΔMTS) was accompanied by a shift in the electrophoretic mobility of endogenous and exogenous HRI, which is indicative of activating autophosphorylation events[17] (Fig. 3b, Extended Data Fig. 9b–d). Consistent with the generation of S-DELE1 being OMA1-dependent, OMA1-deficient cells showed a reduction in the ability of HRI to precipitate wild-type DELE1 after treatment with CCCP, whereas the binding of DELE1(ΔMTS) was unaffected (Extended Data Fig. 9e, f). Given that the TPR domains of DELE1 are probably involved in its interaction with HRI, we next subjected the TPR-containing section of DELE1 to mutagenesis. DELE1 mutants with internal deletions that mapped to the upstream or downstream portion of the TPR-containing segment[12] localized to the mitochondria in unstressed cells, were cleaved and accumulated in the cytosol after CCCP treatment (Extended Data Fig. 9g, h). Although the corresponding DELE1(ΔMTS) mutants recapitulated the constitutive cytosolic localization of DELE1(ΔMTS), they did not co-precipitate HRI at detectable levels and did not induce (Δ246–272) or only minimally induced (Δ386–420) CHOP expression (Extended Data Fig. 9i–l). Conversely, a C-terminal fragment that encompassed the TPR domains 1–7 (DELE1(TPR1–7)) was sufficient for the binding of HRI and induction of CHOP (Extended Data Fig. 9m, n). After stringent

purification from cells that were treated with a single-guide RNA (sgRNA) to deplete HRI, this C-terminal fragment was also able to efficiently interact with HRI that was generated in *Escherichia coli* (Fig. 3c, Extended Data Fig. 9o). Removal of TPR domains from the C terminus of DELE1(TPR1–7) was better tolerated than removal of TPR domains from the N terminus, with respect to HRI co-precipitation and CHOP activation—with the exception of the first TPR domain, the absence of which was compatible with HRI binding but not CHOP induction. As HRI is known to respond to alterations in cellular haem[17], we also tested whether haem would interfere with the ability of HRI to bind DELE1, which we did not observe (Extended Data Fig. 10a–c). Thus, OMA1-activated DELE1 is redistributed to the cytosol, where it interacts with HRI through its TPR domains to induce CHOP.

Conclusion

We have uncovered a proteolytic signalling axis involving OMA1, DELE1 and HRI that constitutes a link between mitochondrial perturbation and the cytosolic ISR (Extended Data Fig. 10d). Several of the stressors that are routed through DELE1 perturb the mitochondrial membrane potential ($\Delta\Psi$), which is known to trigger OMA1[14,15] and might explain the effects of ATP5IF1 and SLC2A1 on this pathway (Fig. 1a, Extended Data Fig. 10e–h): ATP5IF1 counteracts the reversed activity of complex V when membrane potential is lost[18], thus aggravating CCCP-induced depolarization; SLC2A1 is downregulated in cells with a low mitochondrial membrane potential[19]. Loss of the mitochondrial membrane potential depletes mitochondrial ATP[14,20], in line with our observation that DELE1 cleavage was also triggered by inhibitors of oxidative phosphorylation. The ability of cells to cope with mitochondrial perturbation is a key factor that affects lifespan in model organisms, and is likely to contribute to related phenotypes and age-associated diseases in humans[1,2,3,21]. Modulation of the ISR may be a promising strategy to manipulate dysfunctional mitochondria, but this might be complicated by the highly connected nature of the ISR. Using transcriptomic profiling, we found that the cellular response to mitochondrial membrane depolarization was severely blunted in cells that lack DELE1 or HRI, which resembled the effect observed in wild-type cells co-treated with the ISR inhibitor ISRIB[22](Fig. 3d–f). However, ISRIB blocks the downstream effects of eIF2α phosphorylation and is thus unable to selectively inhibit the cellular response to mitochondrial stress. Notably, in DELE1- or HRI-knockout cells, and cells that were treated with ISRIB, CCCP caused a steep upregulation of heat-shock proteins (including HSPA1A, HSPA1B and DNAJB1). This suggests that an alternative stress-response program might be induced in cells that are unable to signal through DELE1–HRI–eIF2α (Fig. 3e, Extended Data Fig. 10i). Altered signalling was also mirrored by an increase in the resilience of cells that are defective in the DELE1–HRI–eIF2α pathway under conditions of mitochondrial depolarization (Fig. 3g, Extended Data Fig. 11a–c), without signs of generally altered mitochondrial physiology (Extended Data Fig. 11d–j). Conversely, cells that were deficient in DELE1 or HRI showed an inferior tolerance of continuous mild mitochondrial perturbation that was caused by the absence of MFN2, suggesting that DELE1 and HRI have a protective function in this context (Extended Data Fig. 11k, l). MFN2 has a central role in mitochondrial dynamics and mitophagy and can cause peripheral neuropathies[13,23]. Of note, the DELE1 biology that we have uncovered here could also be observed in cells of neuronal

origin (Extended Data Fig. 11m–o). Thus, manipulation of the OMA1–DELE1–HRI axis or the additional pathway components identified here could be beneficial in the context of human health under certain settings of mitochondrial malfunction.

Methods

Cell lines and culture

HAP1 cells were cultured in Iscove's modified Dulbecco's medium (IMDM) (Thermo Fisher Scientific) supplemented with 10% heat-inactivated fetal calf serum (FCS) (Thermo Fisher Scientific) and 1% penicillin–streptomycin– glutamine solution (Thermo Fisher Scientific). HEK293T (293T), HeLa and HCT116 cells were maintained in Dulbecco's modified Eagle's medium (DMEM) (Thermo Fisher Scientific) containing the same supplements, as were BJEH and primary fibroblasts (gifts from T. Brummelkamp). SH-SY5Y cells (a gift from V. Hornung) were maintained in DMEM supplemented with 15% FCS, 1% penicillin–streptomycin–glutamine and 1 mM sodium pyruvate. N/TERT-1 keratinocytes[24] (a gift from J. Rheinwald) were maintained in a 1:1 mixture of DMEM and Ham's F12 (Thermo Fisher Scientific) supplemented with 2 mM L-glutamine (Thermo Fisher Scientific), 0.2 ng ml^{-1} epidermal growth factor (EGF), 25 μg ml^{-1} bovine pituitary extract (BPE; Thermo Fisher Scientific), 0.4 mM $CaCl_2$ and 1% penicillin–streptomycin (Thermo Fisher Scientific). Cell lines were tested initially for mycoplasma contamination, but thereafter were not tested routinely.

Generation of endogenously tagged cell lines

To generate HAP1 $CHOP^{Neon}$ cells, haploid HAP1 cells were transfected with a pX330 plasmid (Addgene, 42230) that encodes an sgRNA targeting the last codon of *DDIT3* (CHOP) together with a donor vector containing a cassette consisting of a glycine and serine linker, 3×Flag, mNeon, polyA signal, pause site, human phosphoglycerate kinase (hPGK) promoter, puromycin *N*-acetyltransferase and polyA signal. This cassette was flanked upstream and downstream by a synthetic sgRNA recognition site[25]. Another pX330 plasmid encoding an sgRNA against these synthetic sgRNA recognition sites was included to release the knock-in cassette after uptake into the transfected cells. Transfected cells were expanded and subjected to puromycin selection (1μg ml^{-1}) to enrich for cells that integrated the cassette into the genome. Single cell clones were then derived and analysed for the in-frame integration of the donor cassette into the *DDIT3* locus by PCR and Sanger sequencing. 293T HRI^{Flag} (*EIF2AK1*^{Flag}) cells were created analogously, except that the knock-in vector contained a 3×Flag tag, followed by a cytomegalovirus (CMV)-driven puromycin *N*-acetyltransferase cassette, flanked on both sides by an sgRNA sequence derived from the *Danio rerio tia1l* locus. $DELE1^{HA}$ (*DELE1*^{HA}) 293T cells were generated similarly, except that the donor vector contained a glycine and serine linker and 3×HA tag, flanked on either side by the sgRNA recognition site and homology arms mapping to around 330 bp upstream and downstream of the stop codon at the *DELE1* locus. The sgRNA recognition sequence near the *DELE1* stop codon was eliminated in the donor DNA sequence via synonymous mutations.

Europe PMC Funders Author Manuscripts

Haploid genetic screens for identification of CHOP regulators

Ultra-deep genome-wide mutagenesis of haploid HAP1 cells was carried out as described previously[9]. In brief, an mCherry-containing variant of gene-trap retrovirus[26] was produced in 293T cells and collected for the first time 48 h after transfection, followed by five additional collections every 12 h. Retroviral particles were concentrated by ultracentrifugation at 22,800 rpm for 2 h at 4 °C and stored at 4 °C overnight. To generate random genomic mutations via insertional mutagenesis by the gene-trap virus[27], haploid HAP1 CHOP^{Neon} cells were plated at 15 million cells and transduced with concentrated viral particles 24 h after plating, followed by two additional transductions. The resulting library of mutants was expanded, frozen and used for genetic screens.

To identify CHOP regulators, mutagenized HAP1 CHOP^{Neon} cells were plated at 20% confluence in a total of 20 T175 flasks (Sarstedt) and treated 48 h after plating for 16 h with 20 μM CCCP, or for 9 h with 10 μM tunicamycin or 2.5 μM CDDO (2-cyano-3,12-dioxo-oleana-1,9(11)-dien-28-oic acid). Cells were collected using Trypsin-EDTA (0.25%, Gibco), stopped with full medium and washed with PBS. Dissociated cells were passed through a 40-μm cell strainer (Greiner, 542040) before fixation with one pellet volume of BD fix buffer I (BD Biosciences) for 10 min at 37 °C. Fixation was stopped with PBS containing 1% FCS, and cells were once more passed through a 40-μm cell strainer and counted. Approximately 1.5 × 10^9cells were permeabilized with one pellet volume of cold BD Perm Buffer III (BD Biosciences) for 30 min on ice. Permeabilization was stopped with PBS containing 1% FCS and cells were blocked at 100 million cells per ml in PBS with 1% FCS and 3% bovine serum albumin (BSA) for 30 min at room temperature. The CHOP^{Neon} protein was stained with the anti-mNeonGreen antibody (Chromotek, 32f6-10; for a list of antibodies used in this study see Supplementary Table 5) diluted 1:2,500 in PBS with 1% FCS and 1% BSA for 2.5 h at room temperature on a rotator, followed by three 15-min washing steps with PBS and 1% FCS at room temperature on a rotator. Secondary antibody staining (anti-mouse-AF488, 1:500, Life Technologies) was then performed in PBS with 1% FCS and 1% BSA for 1 h at room temperature on a rotator protected from light. For a DNA counterstain, DAPI (Sigma-Aldrich, D9542) was added to the secondary antibody dilution at a final concentration of 2.5 μg ml^{-1}. After three washing steps as above, cells were resuspended at 100 million cells per ml in PBS and 1% FCS, stored at 4 °C and sorted on a BD Fusion cell sorter (BD Biosciences) using a 70-μm nozzle. Staining specificity was determined using a secondary-antibody-only control. Haploid cells were identified on the basis of DNA content in the DAPI channel and of those, approximately 10^7 cells of the bottom 4% CHOP^{Neon}-low and top 4% CHOP^{Neon}-high cells were sorted into PBS and 10% FCS for isolation of genomic DNA.

Insertion-site mapping and analysis

Genomic DNA was extracted from the sorted cell populations using the QIAamp DNA Mini Kit (Qiagen, 51306). De-crosslinking was performed at 56 °C overnight, and subsequent DNA extraction was performed following the manufacturer's instructions. Gene-trap insertion sites of CHOP^{Neon}-high and -low populations were recovered as described previously[9], except that the single-stranded DNA linkers that were used in the ligation reaction and the primers for the final PCR step contained standard Illumina barcodes to

allow for indexed deep sequencing using two index reads. Amplified libraries were sequenced on a HiSeq1500 (Illumina) with a read length of 50 nt (single-end mode). Demultiplexing of indexed sequencing reactions was performed allowing one mismatch. Reads were aligned to the human genome (hg19) and analysed as described previously[9], except that the removal of genomic regions assigned to overlapping genes and 3′ untranslated regions was omitted. Instead, symbols of overlapping genes were concatenated. In brief, Bowtie[28] was used to align demultiplexed reads to the human genome, allowing one mismatch, followed by mapping to the coordinates of RefSeq protein-coding genes with intersectBED[29]. Although insertional mutagenesis yields viral integrations in both orientations relative to the transcriptional direction of the affected genes, only integrations in the sense orientation were considered disruptive and used for downstream analysis. For the identification of regulators of $CHOP^{Neon}$, per gene the number of unique gene-trap insertion sites in the query gene versus the whole sample was compared between the $CHOP^{Neon}$-high and $CHOP^{Neon}$-low cell populations using a two-sided Fisher's exact test and Benjamini–Hochberg FDR correction. Data were plotted as the combined number of unique mutations identified in the $CHOP^{Neon}$-high and $CHOP^{Neon}$-low population (*x* axis) versus their mutation ratio (high versus low) normalized by the respective sizes of the datasets (*y* axis). Scatter plots were created using Python framework plotly Dash or GraphPad Prism. Venn diagrams were created by filtering the data with SQL commands and plotting it using the Python library matplotlib.

Generation of knockout cell lines

Targeted knockout cell lines were generated using the CRISPR–Cas9 system either by transient transfection or transduction. For the latter approach, 293T cells were transfected with the plasmid pL-CRISPR.EFS.tRFP (Addgene, 57819) containing the sgRNA for a gene of interest, and the lentiviral packaging plasmids pMDLg/pRRE, pRSV-Rev and VSV.G. Cells were transduced following standard procedures and RFP-positive cells were sorted on a Sony SH800Z cell sorter. Alternatively, cells were transiently transfected using pX330 plasmids containing the sgRNA of interest along with vectors encoding either puromycin or blasticidin resistance to allow transient selection of transfected cells. For HAP1, 293T and HeLa cells, clonal progeny was generated and verified by PCR and Sanger sequencing.

Treatments, transfections, transductions and live stains

Cells were treated with CCCP (Sigma-Aldrich, C2759, 20 μM unless stated otherwise), CDDO (MedChemExpress, HY-14909, 2.5 μM), tunicamycin (MedChemExpress, HY-A0098, 10 μM), GTPP (GTPP hexafluorophosphate, MedChemExpress, HY-102007A, 10 μM), oligomycin (CST, 9996L, 10 μM or 25 μM), antimycin (Sigma-Aldrich, A8674, 50 μM), valinomycin (BioTechne, 3373, 0.5 μM), pepstatin A (Enzo, ALX-260-085-M005, 50 μM), 1,10-phenanthroline monohydrate (Sigma-Aldrich, P9375, 500 μM), E-64 (Sigma-Aldrich, E3132, 1 μM), E-64d (Enzo, BML-PI107-0001, 50 μM), zVAD (Z-VADFMK, PeptaNova, 3188-v, 20 μM), 3,4-dichloroisocoumarin (Sigma-Aldrich, D7910, 100 μM), Pefabloc SC Plus (Sigma-Aldrich, 1187360100, 500 μM), ISRIB (Sigma-Aldrich, SML0843, 200 nM), haemin (Sigma-Aldrich, 51280, 20 μM) or cycloheximide (Sigma-Aldrich, C4859, 20 μg ml^{-1}) for the indicated times.

Where indicated, cells were transfected 24 to 36 h before treatment using polyethylenimine (PEI 25000, Polysciences) or Turbofectin (OriGene Technologies). Transductions were performed as described previously[26].

Mitochondrial membrane potential was assessed using 100 nM tetramethylrhodamine (TMRM; Thermo Fisher Scientific) following the manufacturer's instructions.

Immunoprecipitation and immunoblotting

Cells for western blot analysis were seeded and treated as described in the figure legends. To collect cell lysates, cells were washed with PBS and lysed with RIPA or SDS sample buffer. After boiling the samples at 75–99 °C for 10 min, proteins were separated by gel electrophoresis using the Bolt gel electrophoresis system (Thermo Fisher Scientific), following the manufacturer's instructions. Bolt gradient gels (4–12%) were used for routine immunoblot analysis and for analysis of small molecular weight changes proteins were separated using 8% Novex gels. After transfer onto polyvinylidene fluoride (PVDF) membranes, proteins were detected with the indicated antibodies.

Cells for co-immunoprecipitation experiments were seeded in 10-cm dishes and treated as described in the figure legends. Cells were washed with cold PBS and lysed in DISC buffer (30 mM Tris-HCl pH 7.5, 150 mM NaCl, 10% glycerol, 1% Triton X-100) with freshly added protease inhibitor cocktail (cOmplete Protease Inhibitor Cocktail, Roche, 11697498001). Cell lysates were incubated on ice for 20 min and subsequently lysates were cleared twice by centrifugation at 20,000*g* for 15 min at 4 °C. An aliquot of the supernatant was kept as input. The cleared supernatants were incubated with either Strep-Tactin Superflow Plus Beads (Qiagen, 30002) or Anti-Flag M2 Magnetic Beads (Sigma, M8823) for precipitation of StrepTagII- or Flag-containing protein complexes, respectively. Beads were blocked with 3% BSA in PBS for 30 min at 4 °C on a rotator and washed five times with DISC before addition of supernatants. For co-immunoprecipitation of proteins bound to endogenous HRI protein, cleared supernatants were incubated with the anti-eIF2AK1 antibody (Proteintech, 20499-1-AP) at a dilution of 1:1,000 at 4 °C on a rotator overnight. Pierce Protein A agarose beads (Thermo Fisher Scientific, 20334) were then added to the lysates.

After a 2.5-h incubation at 4 °C on a rotator, beads were washed 5 times for 5 min each with DISC buffer. After the last washing step, DISC buffer was removed completely, SDS sample buffer was added, beads were boiled at 99 °C for 10 min and proteins were analysed by western blotting as described above.

For phosphatase treatment of protein lysates, cells were lysed in RIPA buffer (150 mM NaCl, 0.1% SDS, 50 mM TRIS-HCl pH 7.5, 1% Triton X-100, 0.5% sodium deoxycholate) with freshly added protease inhibitor cocktail for 15 min on ice and lysates were cleared by centrifugation at 20,000*g* for 15 min at 4 °C. Then, 26 µl of supernatant was transferred to a microfuge tube and 4 µl 10× FastAP buffer and 10 µl FastAP Thermosensitive Alkaline Phosphatase (Thermo Fisher Scientific, EF0654) or RIPA (for control samples) was added. Samples were incubated at 37 °C for 1 h and the reaction was stopped by the addition of 4× SDS sample buffer. For gel source data, see Supplementary Fig. 1.

EGFP trap purification

For generation of DELE1(TPR1–7)–EGFP and EGFP control protein, sgHRI-treated 293T cells were transfected with plasmids expressing the respective transgenes from a CMV promoter and collected 48 h after transfection. In brief, after two washes with PBS, cells were scraped and snap-frozen in liquid N_2. Frozen pellets were then lysed in high-salt lysis buffer (1 M KCl, 50 mM HEPES-KOH pH 7.2, 10% glycerol, 1% IGEPAL CA-630) supplemented with cOmplete, Mini, EDTA-free Protease Inhibitor Cocktail (Roche, 11836170001). Lysates were sonicated and subjected to Pierce Universal Nuclease for Cell Lysis (Thermo Fisher Scientific, 88700) treatment for 30 min at 4 °C to digest DNA. Lysates were cleared twice by centrifugation for 10 min at 21,000*g*, after which an aliquot of each lysate was set aside as input and the remainder was incubated with 40 µl of GFP-TRAP Magnetic Agarose beads (Chromotek, gtma-20) for 2 h at 4 °C. After immunoprecipitation, beads were washed three times with high-salt buffer (0.5 M KCl, 50 mM HEPES-KOH pH 7.2, 10% glycerol), followed by three washes using DISC buffer. A fraction of bead-purified protein was put aside and the remaining beads were combined with 1.6 µg of recombinant GST-HRI protein produced in *E. coli* (Abnova, P5769) per reaction and incubated in DISC buffer at 4 °C overnight. The supernatant was collected and beads were washed six times with DISC buffer, before addition of sample buffer and analysis by SDS–PAGE, along with the immunoprecipitation supernatant and GST–HRI input (85% of the immunoprecipitate was subjected to analysis by Coomassie stain; 5%, 2.5% and 1.25% of the immunoprecipitate, supernatant and GST–HRI input, respectively, were used for immunoblot analysis). The cell lysate input was analysed analogously before and after exposure to GFP-TRAP beads to assess purity. SDS gels were either stained for 1 h using InstantBlue Coomassie Protein Stain (Expedon, ISB1L) or subjected to immunoblotting. In the latter case, DELE1(TPR1–7)–EGFP and EGFP were detected using a rat anti-GFP antibody (Chromotek, 3h9) different from the alpaca nanobody conjugated to the GFP-TRAP beads, whereas GST–HRI was detected using an antibody directed against GST (GE Healthcare, 27457701V).

Crystal violet staining

Cells for staining were seeded in 6-well or 96-well plates and treated as described in the figure legends. Next, cells were fixed by adding 3.7% paraformaldehyde (PFA) for 10 min, washed twice with PBS and stained with crystal violet solution (12.25 mM crystal violet (Carl Roth, T123.1), 20% methanol) for 20 s. Staining solution was washed off with water and plates were dried at room temperature.

Analytical flow cytometry

For analysis of $CHOP^{Neon}$ fluorescence or mitochondrial membrane potential after treatment, cells were detached using Trypsin-EDTA (0.25%, Gibco) and measured on a BD LSRFortessa flow cytometer (BD Biosciences). Data were analysed using BD FACSDiva (BD Biosciences) or FlowJo software (BD).

For transient transfection of HAP1 $CHOP^{Neon}$ cells with cDNAs of interest, mCherry was co-transfected to identify transfected cells. Gating was performed as follows. To identify transfected cells, the top 10% of mCherry-positive cells were gated and their mean mNeon

intensity was divided by the mean mNeon intensity of untransfected (mCherry-negative) cells. For analysis of genetic LONP1 ablation, $CHOP^{Neon}$ cells were seeded in 12-well plates and transduced with a lentiviral construct encoding TagRFP and an sgRNA targeting the indicated genes or a non-targeting control sgRNA. Cells were cultured for 9 days and the levels of $CHOP^{Neon}$ in $TagRFP^{+}$ cells were analysed by flow cytometry. For fitness assays, cells were seeded in triplicates into 12-well plates and separately infected with a lentiviral construct encoding TagRFP and an sgRNA targeting the indicated genes or a non-targeting control sgRNA. The percentage of $TagRFP^{+}$ sgRNA-containing cells was followed over time and normalized to the non-targeting sgRNA control and day 0 measurements.

Immunofluorescence

Cells were seeded at 20% confluence on poly-L-lysine-coated glass cover slips or in µ-Slide chambered coverslips (ibidi, 80826). Between 24 and 36 h after transfection, cells were pre-stained with 100 nM MitoTracker Red (Molecular Probes MitoTracker Red CMXRos, Thermo Fisher Scientific, M7512) for 1 h where indicated and subjected to drug treatments. Where indicated, cells were washed with PBS and stained with WGA647 (Thermo Fisher Scientific, W32466) diluted 1:2,000 in PBS for 5 min at room temperature. Cells were washed with PBS and fixed with 3.7% PFA for 10 min at room temperature. After fixation, cells were washed twice with PBS and permeabilized with 0.05% Triton-X 100 in PBS for 30 min at room temperature, washed twice with PBS and blocked in 10% normal goat serum (NGS; VWR, UPTIUP379030) in PBS for 30 min at room temperature. For visualization of the respective proteins, cells were incubated with primary antibodies in 10% NGS in PBS for at least 1 h at room temperature. After washing three times with PBS, fluorophore-conjugated secondary antibodies were diluted in 10% NGS in PBS and applied for 1 h at room temperature in the dark. Cells were washed three times with PBS (second wash containing 1 µg ml^{-1} DAPI when required) and coverslips were mounted with Roti-Mount FluorCare (Carl Roth HP19.1). Imaging was performed with a Zeiss Observer.Z1 confocal microscope (Carl Zeiss) equipped with a 63× oil immersion objective. Images were obtained using the ZEN 2009 software (Carl Zeiss). Where indicated, imaging was performed with a Leica DMi8 light microscope (Leica) and images were obtained using the LasX software (Leica). All images were analysed using Fiji[30].

Isolation of mitochondria, in vitro FCCP treatment and electron microscopy

Mitochondria from 293T cells were isolated as previously described[31]. In brief, cells from one 15-cm dish were resuspended in 1.0–1.5 ml isolation buffer (300 mM sucrose, 5 mM TES, 200 µM EGTA, pH 7.2). One millilitre of this cell suspension was pumped three times through the cell homogenizer (6-µm clearance) with a constant rate of 1,000 µl min^{-1} and subsequently transferred to a 2-ml microfuge tube. Thereafter 1 ml of isolation buffer was pumped one time (6-µm clearance, 1,000 µl min^{-1}) through the cell homogenizer and transferred to the 2-ml tube. This procedure was repeated for the remaining cell suspension.

The homogenate was centrifuged at 800*g* for 5 min at 4 °C, the supernatant was transferred to a fresh 2 ml microfuge tube and the pellets were resuspended in 150 µl 2× Lämmli buffer, frosted in liquid nitrogen and stored at −80 °C for immunoblot analysis. Then, the supernatant was centrifuged at 10,000*g* for 10 min at 4 °C and 150 µl of the supernatant was

transferred to a 1.5-ml microfuge tube, mixed with 150 µl 2× Lämmli, frosted in liquid nitrogen and stored at −80 °C for immunoblot analysis. The rest of the supernatant was discarded and the pellets (mitochondria) were resuspended in isolation buffer. Protein concentration was determined by the Bradford assay[32] and subsequently adjusted to 2 µg µl $^{-1}$ with isolation buffer. Around 30–120 µl of this suspension was used for in vitro FCCP treatment. The remaining mitochondria were centrifuged at 10,000*g* for 10 min at 4 °C and resuspended in 2× Lämmli with a concentration of 2 µg µl^{-1}, frosted in liquid nitrogen and stored at −80 °C for immunoblot analysis.

The mitochondrial transmembrane potential was determined as described previously[33]. The assay was performed in black 96-well plates, and per well 30 µl of mitochondria (2 µg µl^{-1}) was mixed either with 50 µl of 500 nM rhodamine 123 (Invitrogen, R302), 50 µl 0.02% DMSO and 70 µl of swelling buffer (200 mM sucrose, 10 mM MOPS-Tris, 5 mM succinate (Merck, 8.20151.0100), 5 mM pyruvate (Sigma-Aldrich, P2256), 2 mM malate (Sigma-Aldrich, 02288), 1 mM H_3PO_4 and 10 µM EGTA) or with 50 µl 500 nM rhodamine 123, 50 µl 2µM FCCP (final concentration of 500 nM; in 0.02% DMSO; Sigma-Aldrich, C2920) and 70 µl of swelling buffer. Membrane potential was measured for 1 h at 37 °C (excitation 495/15, emission 537/10) in a multiplate reader. Subsequently, 100 µl from each well was transferred to a 1.5-ml microfuge tube and centrifuged at 10,000*g* for 10 min at 4 °C. The supernatant was transferred to a fresh 1.5-ml microfuge tube and mixed with an equal amount of 2× Lämmli. The pellet was resuspended in 15 µl 2× Lämmli. In case of replicates, the samples were pooled and the amount of added 2× Lämmli was adjusted accordingly. Samples were frosted in liquid nitrogen and stored at −80 °C for immunoblot analysis.

Electron microscopy of isolated mitochondria was done as previously described[34]. Samples were fixed with 2.5% glutaraldehyde in 0.1 M sodium cacodylate buffer, pH 7.4 (Electron Microscopy Sciences) for a minimum of 24 h. After this, the glutaraldehyde was removed and samples were washed three times with 0.1 M sodium cacodylate buffer, pH 7.4. Post-fixation and pre-staining treatment was done for 45 to 60 min with 1% osmium tetroxide (10 ml 4% osmium teroxide (Electron Microscopy Sciences, 19190), 10 ml double-distilled H_2O, 10 ml 3.4% sodium chloride and 10 ml 4.46% potassium dichromate (pH adjusted to 7.2 with KOH (Sigma Aldrich)). Samples were washed three times with double-distilled H_2O and dehydrated with an ascending ethanol series (15 min with 30%, 50%, 70%, 90% and 96%, respectively, and three times 10 min with 100%) and propylene oxide (two times 30 min, Serva Electrophoresis GmbH). Samples were then embedded in Epon (3.61 M glycidether 100 (Serva Electrophoresis GmbH), 1.83 M methylnadicanhydride (Serva Electrophoresis GmbH), 0.92 M dodecenylsuccinic anhydride (Serva Electrophoresis GmbH) and 5.53 mM 2,4,6-tris(dimethylaminomethyl)phenol (Serva Electrophoresis GmbH)). Ultrathin sections were automatically stained with UranyLess EM Stain (Electron Microscopy Sciences) and 3% lead citrate (Leica) using the contrasting system Leica EM AC20 (Leica) and examined with an JEOL 1200 EXII transmission electron microscope (JEOL GmbH).

Seahorse measurements

Mitochondrial function was assessed using the Agilent Seahorse XF Cell Mito Stress Test Kit and Seahorse XFe96 FluxPak (Agilent Technologies, 103015-100 and 102601-100), and the oxygen consumption rate was monitored with the Seahorse XFe96 Analyzer (Agilent Technologies) following the manufacturer's instructions. HeLa cells (2×10^4) of the indicated genotypes were seeded in a 96-well plate on the day before the assay including four to six replicate culture wells per run. One hour before the assay, cells were washed twice with Seahorse XF DMEM medium (Agilent Technologies, 103575-100) followed by addition of 180 µl Seahorse XF DMEM medium per well, supplemented with 1 mM pyruvate, 2 mM glutamine and 10 mM glucose (Agilent Technologies, 103578-100, 103579-100 and 103577-100). Subsequently, cells were placed in a CO_2-free BioTek Cytation 1 imaging reader, in which bright-field images of each well were taken. The mito-stress test was performed following the standard protocol. For oligomycin and rotenone plus antimycin A (Rot/AA) the recommended concentrations of 1.5 µM and 0.5 µM, respectively, were used. The optimal FCCP concentration was determined by titration from 0.125 to 1 µM and was found to be 250 nM. To determine cell numbers, Hoechst 33342 (Thermo Fisher Scientific, 62249) was added to the rotenone plus antimycin A dilution to reach a final concentration of 8 µM. After completion of the mito-stress test, cells were returned to the BioTek Cytation 1 imaging reader, in which fluorescence images of the Hoechst 33342 signal were taken. The resulting cell numbers were imported into the Wave 2.6.1 software and normalization was applied. The Seahorse XF Mito Stress Test Report Generator 4.03 was used for analysis.

RNA sequencing

HAP1 wild-type and clonal knockout cells were plated on the day before treatment in 6-well plates. On the next day, cells were treated with CCCP and/or ISRIB as indicated for 12 h. Per condition, two independent clones were treated in two replicates each. Cells were then washed once with PBS and lysed in TRIzol reagent (Thermo Fisher Scientific, 15596018) on ice. Lysates were transferred to microfuge tubes, snap-frozen in liquid nitrogen and stored at −80 °C.

RNA of 300 µl TRIzol lysate was isolated using the Maxwell RSC miRNA Tissue Kit (Promega, AS1460) following the manufacturer's instructions. Afterwards, the RNA concentration was quantified (NanoDrop, Thermo Fisher Scientific) and 1 µg of isolated RNA was also purified using Agencourt RNAClean XP Beads (Beckman Coulter, A63987). The purified RNA was quantified and quality controlled (Bioanalyzer, Agilent). For generating sequencing libraries, 500 ng high-quality RNA (RNA integrity number (RIN) > 8.0) was processed using the SENSE mRNA-Seq Lib Prep Kit V2 (Lexogen, A01161). Sequencing was performed using a HiSeq1500 instrument (Illumina) with a read length of 50 nt, single-end mode. Transcriptome data were analysed using the Galaxy web interface[35]. After demultiplexing and recommended trimming, the data was mapped against the human genome (hg19) using RNA-STAR mapper (Galaxy v.2.5.2b-0). The abundance of mapped reads was analysed using HTseq-count (Galaxy v.1.0.0). Afterwards, a differential gene expression analysis based on the negative binominal distribution was performed based on four replicates per condition (two independent clones treated in duplicates) using DESeq2

(Galaxy v.2.11.39) setting the FDR to less than 0.05 (ref. 36). The DESeq2 output is provided in Supplementary Tables 6–10.

For hierarchical clustering, genes with an FDR-adjusted *P* value < 10^{-12} and a $|\log_2$-transformed fold change| > 1.5 in at least one of the datasets were considered. Clustering was performed using Cluster 3.0 (ref. 37), with an uncentred correlation as distance measure and complete linkage clustering as clustering method. The results were visualized using Java TreeView v.1.1.6r4 (ref. 38). A list of ATF4 and CHOP targets was compiled by combining annotated ATF4 and CHOP target genes[39] with data on ATF4-binding sites[40]. Heat-shock proteins were derived by Gene Ontology analysis[41,42,43]. Significant enrichment of gene collections (ATF4 and CHOP target genes, and heat-shock proteins) among clusters was calculated using a two-sided Fisher's exact test, followed by FDR correction. Densities on the heat map were defined as two divided by the sum of distances to the left and right neighbour (the distance of two directly adjacent genes being one unit). For genes at the edge, the distance to their only neighbour was doubled. Volcano plots were assembled using the unfiltered DESeq2 output of the complete data and plotted using Python framework plotly Dash.

Cloning of cDNAs

The coding sequences of genes expressed in this study were amplified from human cDNA. The coding sequence of MFN2 was amplified from MFN2-YFP (Addgene, 28010). All primer sequences are listed in Supplementary Table 4. Amplified DNA was subjected to restriction digest and ligation using standard cloning procedures. All cloned constructs were sequence-verified by Sanger sequencing.

Statistics and reproducibility

For genome-wide genetic screens, 2.12 × 10^7 (CCCP), 2.07 × 10^7 (tunicamycin) and 1.90 × 10^7(CDDO) individual single cells were interrogated phenotypically by fluorescence and genetically by deep sequencing. This yielded a total of 5,579,161 unique sense mutations (averaging 297 unique mutations per identified gene) for the CCCP data, 4,883,298 (averaging 262 per gene) for the tunicamycin data and 4,286,443 (averaging 232 per gene) for the CDDO data. Per experiment, a two-sided Fisher's exact test was used to calculate enrichment of mutations in the high or low channel and *P* values were FDR-corrected using the Benjamini–Hochberg method[9].

For analytical flow cytometry data, unless stated otherwise in the figure legend, data represent the mean ± s.d. of $n = 3$ biologically independent experiments, with each experiment containing triplicate specimens (that is, separately cultured and treated cell populations). Statistical significance was assessed as described in the figure legends using GraphPad Prism 8.

For immunoblotting data, unless stated otherwise in the figure legend, data are representative of $n = 3$ biologically independent experiments with similar results. For quantification of immunoblot data, statistical significance was assessed using GraphPad Prism 8 with the

appropriate type of analysis (that is, *t*-test for a single comparison and ANOVA for multiple comparisons) and false discovery correction, as indicated in the figure legends.

For microscopy experiments, unless stated otherwise in the figure legend, data are representative of $n = 3$ biologically independent experiments with similar results.

A detailed account of the processing and statistical analysis of RNA sequencing (RNA-seq) data is provided in the 'RNA sequencing' section.

No statistical methods were used to predetermine sample size. The experiments were not randomized, and investigators were not blinded to allocation during experiments and outcome assessment.

Europe PMC Funders Author Manuscripts

Europe PMC Funders Author Manuscripts

Extended Data

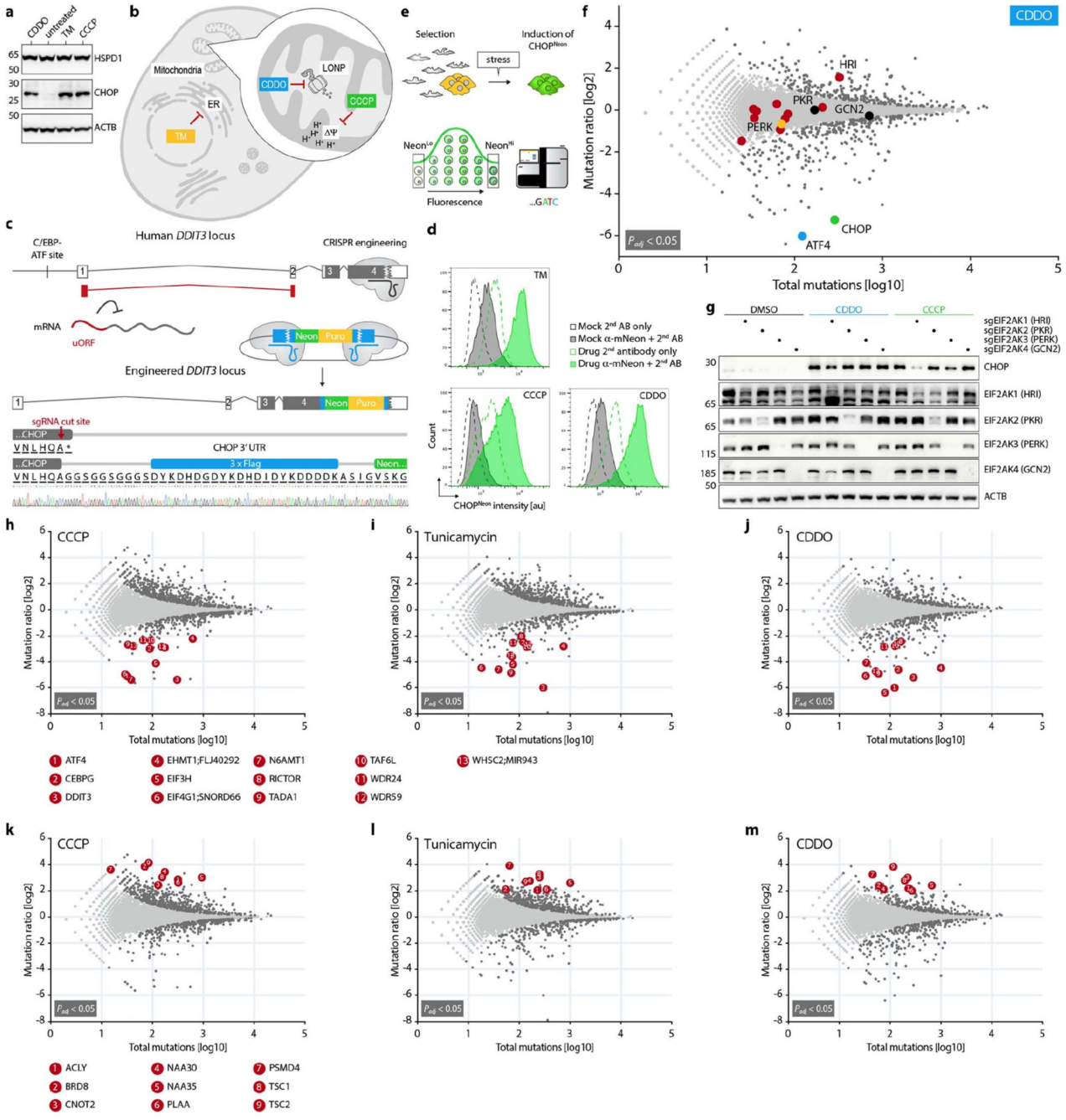

Extended Data Fig. 1. CHOP and CHOP^{Neon} protein levels in the context of different types of pharmacological stimulation.

a, Wild-type HAP1 cells were treated as indicated for 9 h and analysed by immunoblotting. TM, tunicamycin. **b**, Schematic depicting the expected cellular activities of CCCP, tunicamycin and CDDO. ER, endoplasmic reticulum; LONP, LON protease 1; $\Delta\Psi$, mitochondrial membrane potential. **c**, CRISPR engineering of the *DDIT3* locus, resulting in an endogenous in-frame fusion of CHOP with a triple Flag tag followed by mNeon as

indicated. **d**, Pharmacological stimulation of wild-type HAP1 $CHOP^{Neon}$ cells for 9 h (tunicamycin and CDDO) or 16 h (CCCP) leads to induction of the $CHOP^{Neon}$protein, which was measured by flow cytometry (one representative experiment shown of three independent experiments). **e**, Schematic depicting the generation of $CHOP^{Neon}$ cells and their interrogation in phenotypic genetic screening after exposure to cellular stress. Mutagenized cells were sorted on the basis of mNeon intensity ($Neon^{Lo}$ and $Neon^{Hi}$ populations) and gene-trap mutations in these populations were analysed by deep sequencing. **f**, Regulators of $CHOP^{Neon}$ in the genome-wide screen using CDDO ($n = 1.90 \times 10^7$ interrogated single cells). Genes are coloured as in Fig. 1a, b, with dark grey denoting significant enrichment for mutations (two-sided Fisher's exact test, FDR-corrected *P* value (P_{adj}) < 0.05). The two other eIF2α kinases GCN2 (encoded by *EIF2AK4*) and PKR (encoded by *EIF2AK2*) are also highlighted in black. **g**, HAP1 cells were exposed to sgRNAs that target one of the four eIF2α kinases, pharmacologically stimulated for 9 h as indicated and assayed for CHOP induction by immunoblotting (one representative experiment shown of two independent experiments). **h**–**m**, Common regulators of $CHOP^{Neon}$ in the genome-wide screens using CCCP, tunicamycin or CDDO. Data are from Fig. 1a, b and panel **f**, with the statistical significance of mutation enrichment assessed and visualized in the same way. Genes that were identified as significant positive regulators (P_{adj} < 0.05) with a mutation ratio lower than 0.25 (**h**–**j**) or negative regulators with a mutation ratio higher than 4 (**k**–**m**) and which are shared across all three datasets are highlighted in red. *WHSC2* is also known as *NELFA*.

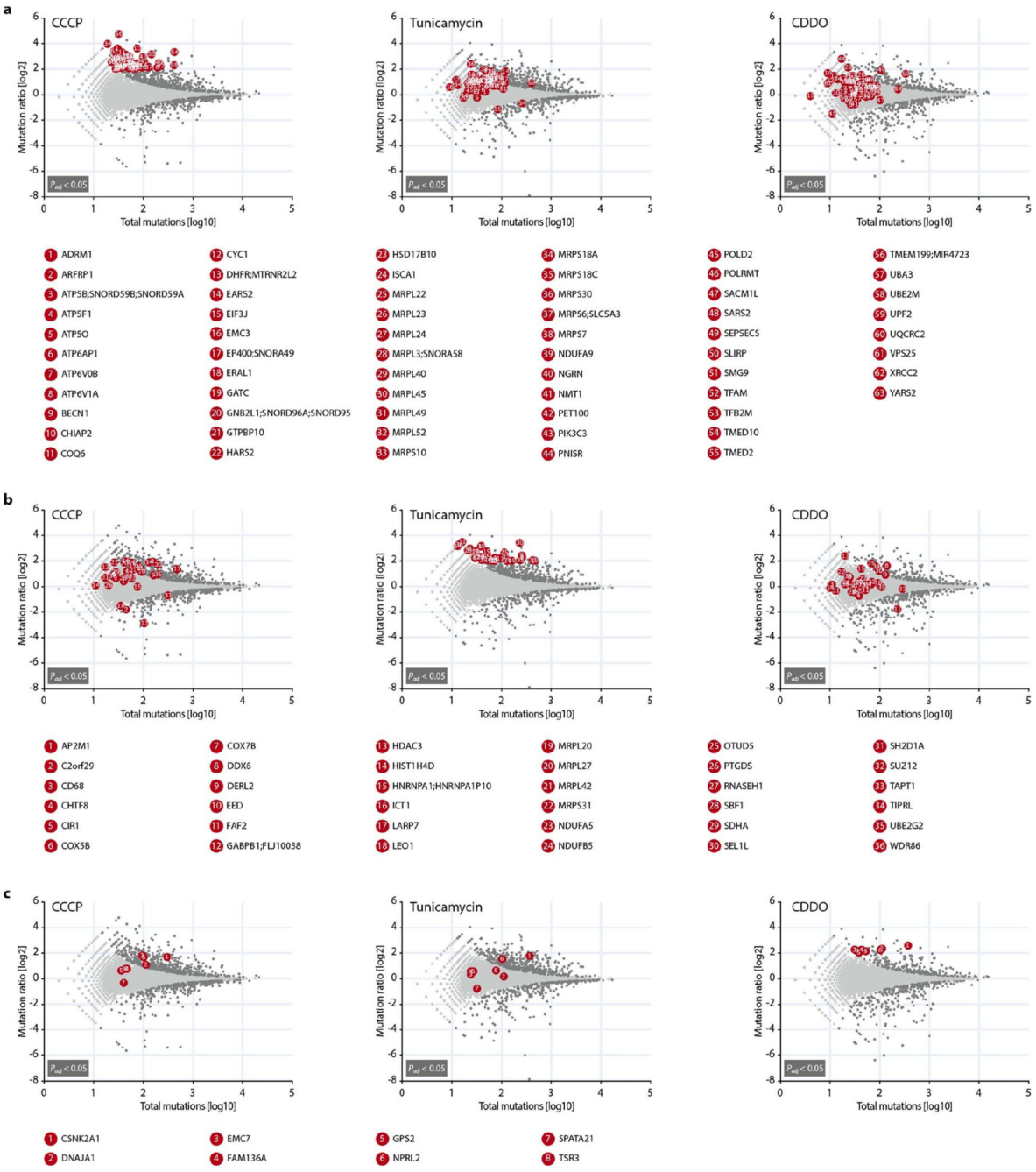

Extended Data Fig. 2. Unique negative regulators of CHOP^{Neon} across genetic screens.

a–**c**, Data from Fig. 1a, b and Extended Data Fig. 1f, with statistical significance of mutation enrichment assessed and visualized in the same way. Genes that were identified as significant negative regulators (two-sided Fisher's exact test, $P_{adj} < 0.05$) and which had a mutation ratio higher than 4 in the query dataset but not in either of the other two datasets are highlighted in red: CCCP versus tunicamycin and CDDO (**a**); tunicamycin versus CDDO and CCCP (**b**); CDDO versus CCCP and tunicamycin (**c**). *ATP5B* is also known as

Europe PMC Funders Author Manuscripts

Europe PMC Funders Author Manuscripts

ATP5F1B; *ATP5F1* as *ATP5PB*; *ATP5O* as *ATP5PO*; *GNB2L1* as *RACK1*; *C2or f29* as *CNOT11*; *HIST1H4D* as *H4C4*; and *ICT1* as *MRPL58*.

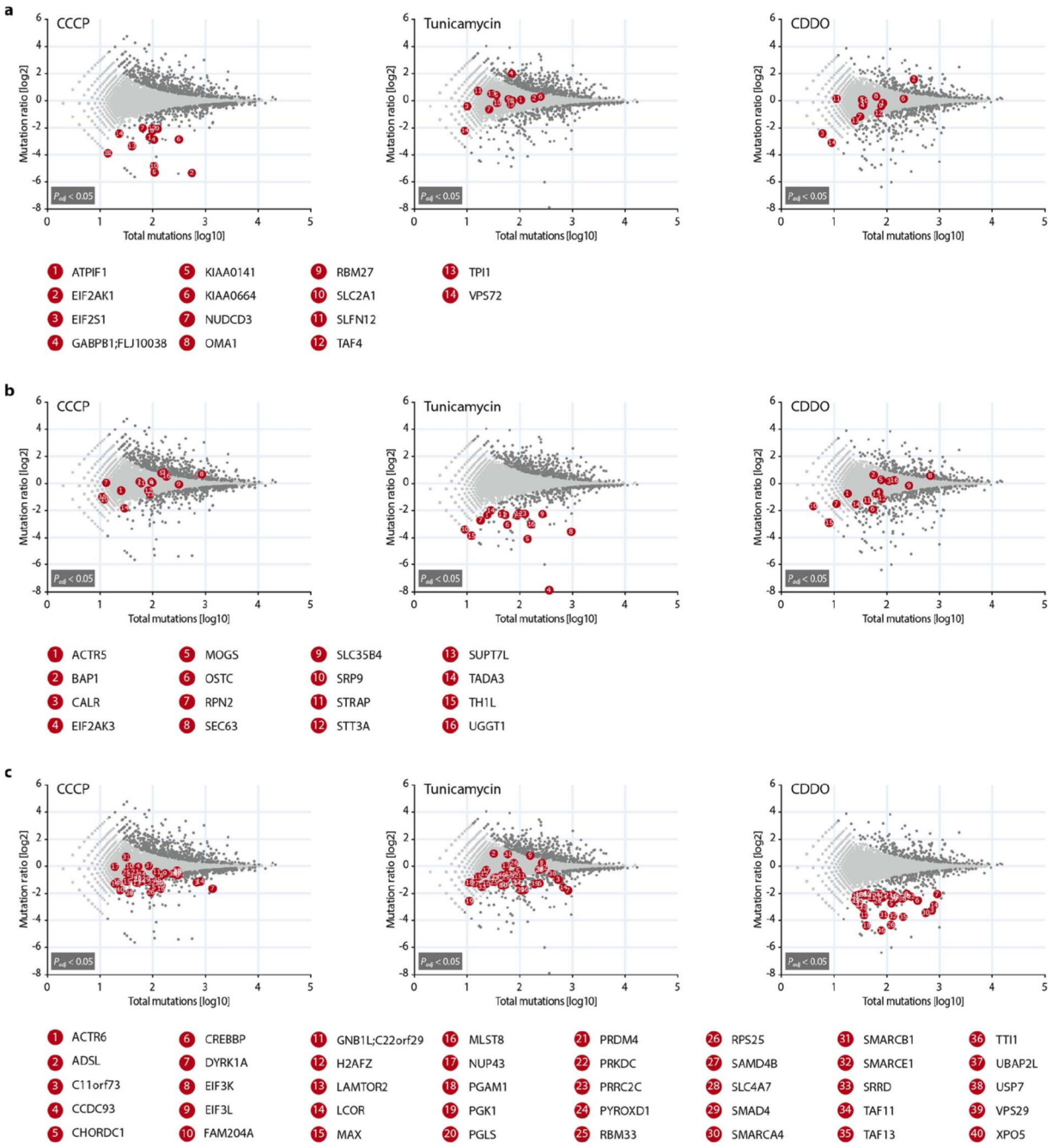

Extended Data Fig. 3. Unique positive regulators of CHOP^{Neon} across genetic screens.

a–c, Data from Fig. 1a, b and Extended Data Fig. 1f, with statistical significance of mutation enrichment assessed and visualized in the same way. Genes that were identified as significant positive regulators (two-sided Fisher's exact test, $P_{adj} < 0.05$) and which had a mutation ratio lower than 0.25 in the query dataset but not in either of the other two datasets

are highlighted in red: CCCP versus tunicamycin and CDDO (**a**); tunicamycin versus CDDO and CCCP (**b**); CDDO versus CCCP and tunicamycin (**c**). *ATPIF1* is also known as *ATP5IF1*; *KIAA0141* is also known as *DELE1*; *KIAA0664* is also known as *CLUH*; *TH1L* is also known as *NELFCD*; *C11orf73* is also known as *HIKESHI*; *C22orf29* is also known as *RTL10*; *H2AFZ* is also known as *H2AZ1*.

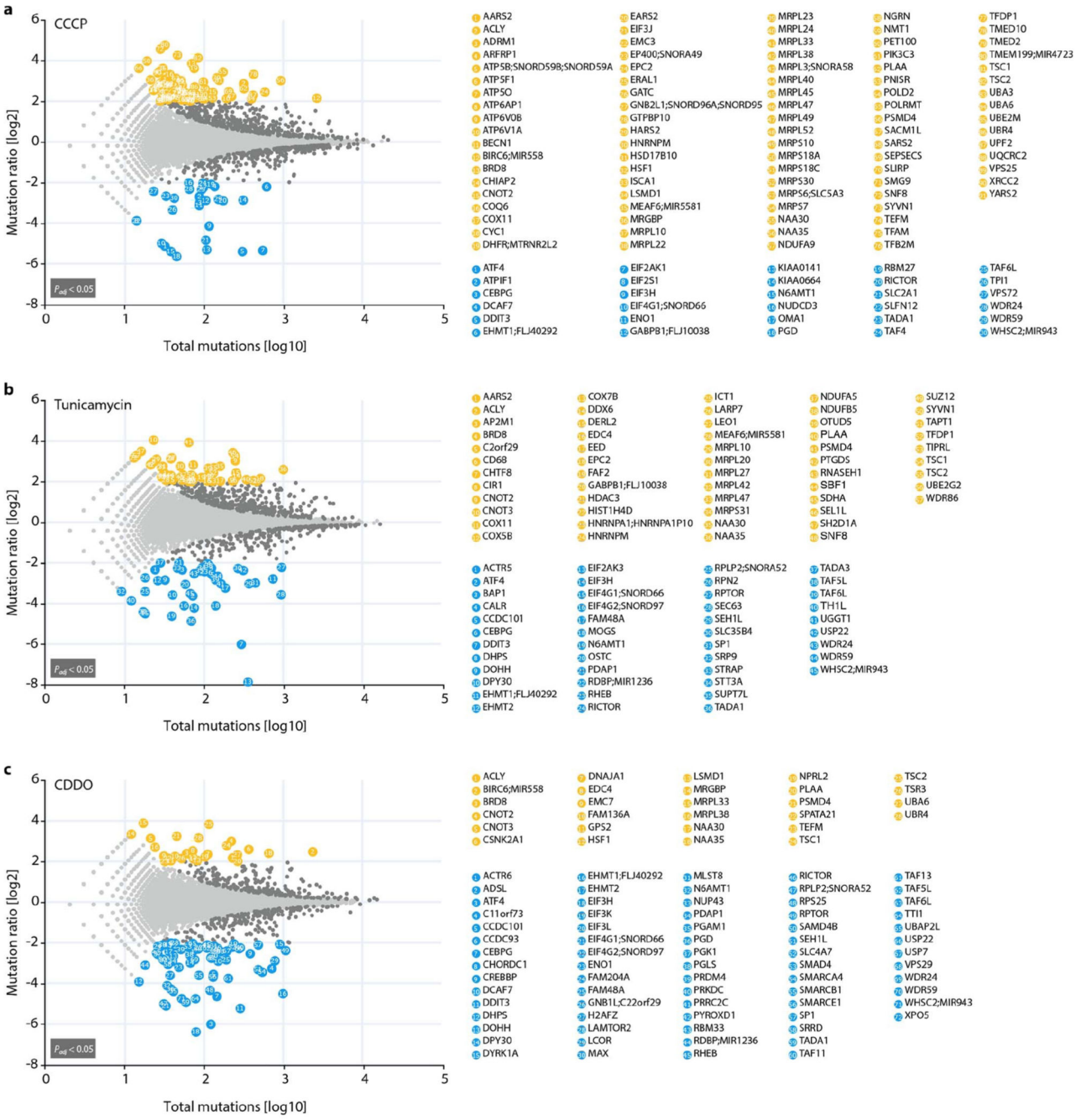

Extended Data Fig. 4. Overview of positive and negative regulators of CHOP^{Neon}after treatment with different drugs.

Europe PMC Funders Author Manuscripts

a–**c**, Data from Fig. 1a, b and Extended Data Fig. 1f, with statistical significance of mutation enrichment assessed and visualized in the same way. For all datasets, significant positive regulators (two-sided Fisher's exact test, $P_{adj} < 0.05$) with a mutation ratio lower than 0.25 (corresponding to an effect size of 4× or greater) are shown in blue, whereas significant negative regulators (two-sided Fisher's exact test, $P_{adj} < 0.05$) with a mutation ratio higher than 4 are shown in yellow.

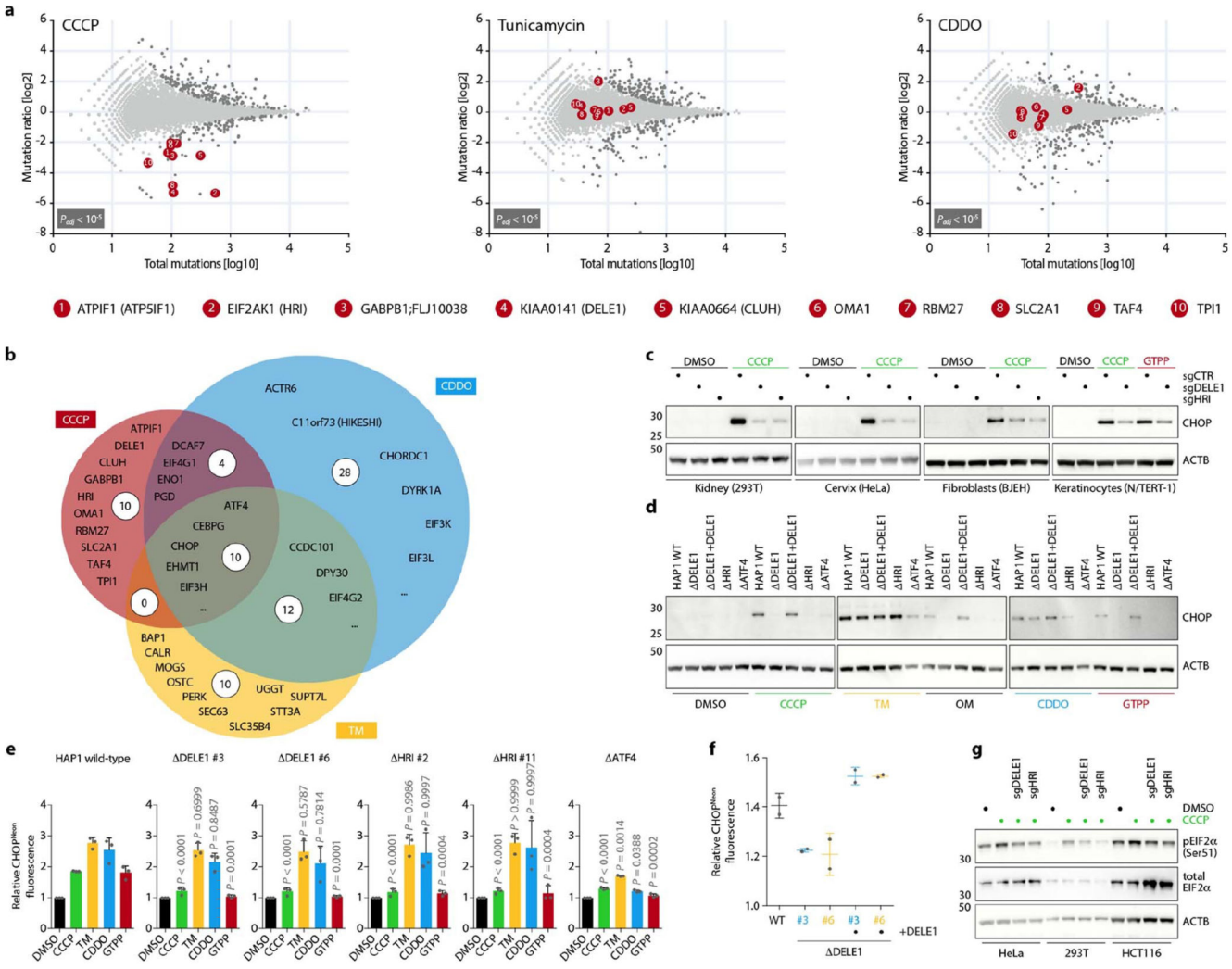

Extended Data Fig. 5. Intersection of the most pronounced positive regulators of CHOP^{Neon} across genetic screens and validation of DELE1 and HRI as mediators of mitochondrial stress.

a, Data from Fig. 1a, b and Extended Data Fig. 1f, processed in the same way, except that genes that were identified as highly significant positive regulators (two-sided Fisher's exact test, $P_{adj} < 10^{-5}$) with a mutation ratio lower than 0.25 in the CCCP dataset but not in either of the other two datasets are highlighted in red. **b**, Venn diagram showing the results of stringent filtering of positive CHOP^{Neon} regulators from **a** (two-sided Fisher's exact test, $P_{adj} < 10^{-5}$ and mutation ratio lower than 0.25) as intersections between all three of the genetic screens that were performed in this study. *CCDC101* is also known as *SGF29*. **c**,

HeLa cells, 293T cells, BJEH fibroblasts and N/TERT-1 keratinocytes were exposed to sgRNAs directed against the specified genes and pharmacologically stimulated for 9– 12 h before immunoblotting (one representative experiment shown of $n = 2$ (HeLa and 293T) or $n = 3$ (BJEH and N/TERT-1) independent experiments). sgCTR, non-targeting control sgRNA. **d**, Clonal HAP1 knockout and stably reconstituted cells were treated as indicated (CCCP, tunicamycin and oligomycin (OM), 9 h; CDDO and GTPP, 11 h) and analysed by immunoblotting. **e**, HAP1 $CHOP^{Neon}$ cells of the indicated genotypes were treated for 9 h (CCCP, tunicamycin, CDDO) or 12 h (GTPP) and analysed by flow cytometry. Per genotype and treatment, the $CHOP^{Neon}$signal was normalized to its DMSO control and statistical significance is indicated compared to identically treated wild-type cells (mean ± s.d. of $n = 3$ independent experiments; one-way ANOVA with Dunnett's multiple comparisons correction). **f**, Wild-type, DELE1-deficient (clones #3 and #6) and stably reconstituted HAP1 $CHOP^{Neon}$ cells were transduced with lentiviral constructs that contain a non-targeting control sgRNA or an sgRNA directed against *LONP1*. $CHOP^{Neon}$ levels were analysed by flow cytometry. Per genotype, the $CHOP^{Neon}$ fluorescence detected in sgLONP1-treated cells is shown relative to the $CHOP^{Neon}$ fluorescence detected in the matching sgCTR-treated cells ($n = 2$ independent experiments). **g**, HeLa, 293T and HCT116 cells—either wild type or that were transiently exposed to an sgRNA directed against *EIF2AK1* (HRI) or *DELE1*—were stimulated with CCCP for 1 h and the phosphorylation of eIF2α was analysed by immunoblotting (one representative experiment shown of two independent experiments).

Europe PMC Funders Author Manuscripts

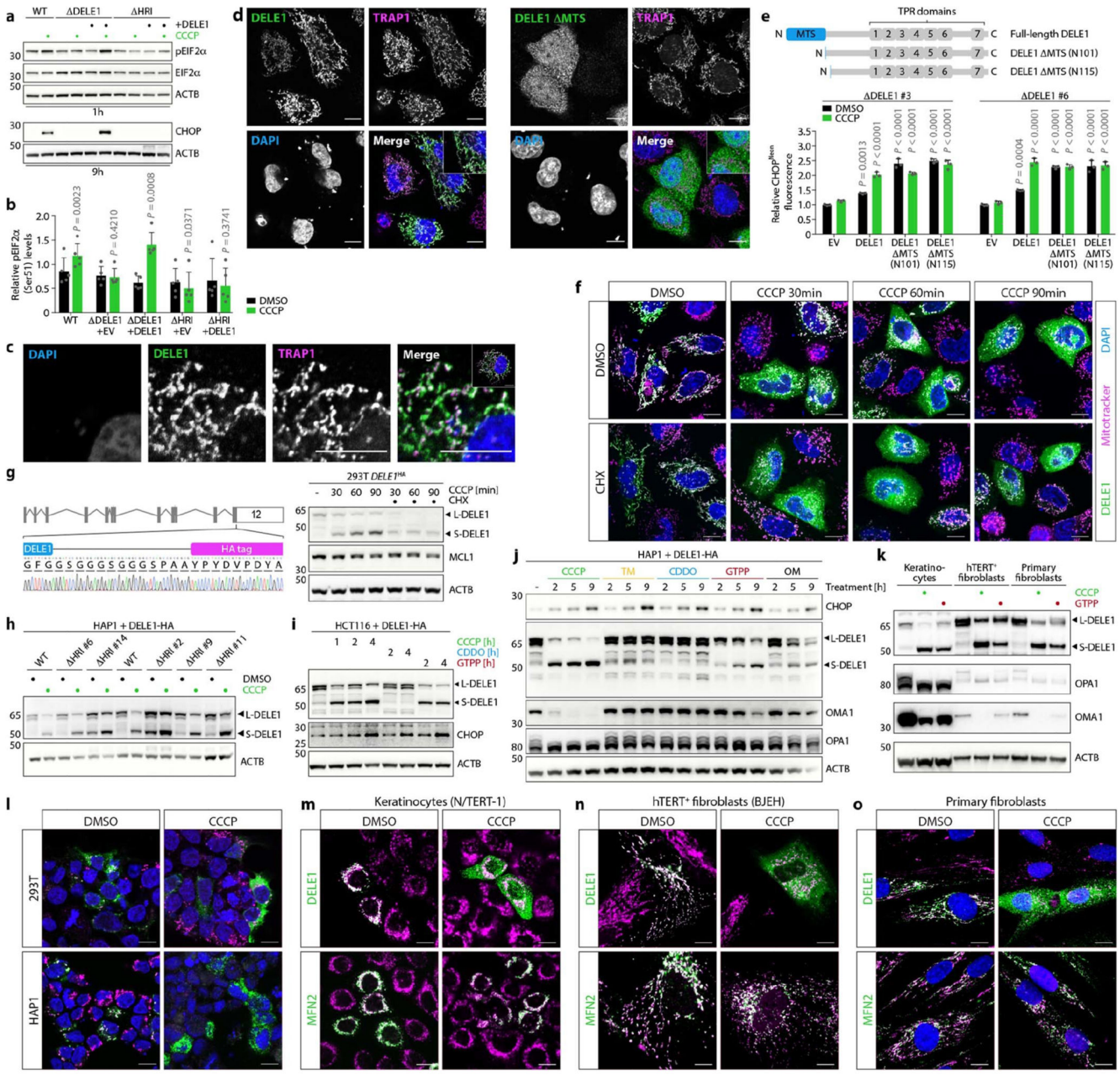

Extended Data Fig. 6. DELE1 operates upstream of HRI, is cleaved and accumulates in the cytosol across different types of mitochondrial perturbation and different cellular systems.

a, **b**, HeLa wild-type, knockout and stably reconstituted cells were treated for 1 h (phosphorylated eIF2α) or 9 h (CHOP) with CCCP. Cells were analysed by immunoblotting (**a**) and the levels of phosphorylated eIF2α were quantified relative to ACTB (**b**; mean ± s.d. of $n = 5$ independent experiments; for each genotype, CCCP treatment was compared to DMSO using a paired two-tailed Student's *t*-test). **c**, **d**, Subcellular localization of HA-tagged DELE1 or DELE1(ΔMTS) in HeLa cells analysed by confocal microscopy. TRAP1 staining identifies mitochondria and nuclei were visualized with DAPI. **e**, Top, clonal DELE1-knockout HAP1 CHOP^{Neon} cells were transiently transfected with full-length

DELE1 or truncation mutants that lack the first 101 (DELE1(ΔMTS(N101))) or 115 (DELE1(ΔMTS(N115))) amino acids as indicated. Bottom, transfected cells were treated with CCCP or DMSO for 9 h and analysed by flow cytometry as in Fig. 2a (mean ± s.d. of n = 3 independent biological samples; two-way ANOVA with Tukey's multiple comparisons correction; one representative experiment shown of three independent experiments). **f**, HeLa cells were transfected with DELE1-HA, treated with CCCP alone or CCCP and cycloheximide (CHX) as indicated and analysed for subcellular localization of DELE1. Mitochondria were stained with MitoTracker and nuclei were visualized using DAPI. **g**, CRISPR engineering of the *DELE1* locus in 293T cells (introducing a C-terminal in-frame fusion with a triple HA tag), followed by treatment with CCCP alone or CCCP and cycloheximide and analysis by immunoblotting (one representative experiment shown of four independent experiments). **h**, Wild-type and HRI-knockout HAP1 cells were transfected with DELE1-HA and treated as indicated. The fate of the DELE1–HA protein was analysed by immunoblotting (n = 5 (HRI) or 2 (wild type) biologically independent clones). **i**, **j**, HCT116 (**i**) and HAP1 (**j**) cells were transfected with DELE1-HA, treated with the specified compounds and analysed for DELE1– HA cleavage and CHOP induction by immunoblotting (one representative experiment shown of two independent experiments). **k**, N/TERT-1 keratinocytes, hTERT^{+} (BJEH) fibroblasts and primary fibroblasts were transduced with DELE1–HA, stimulated for 4 h as indicated and assayed by immunoblotting. **l**, Wild-type 293T and HAP1 cells were transfected with DELE1-HA and treated with CCCP for 4 h. The localization of DELE1–HA was analysed as in Fig. 2d (one representative experiment shown of two independent experiments). **m**–**o**, Cells from **k** were stimulated as indicated for 4 h and the localization of DELE1–HA and MFN2 were analysed by confocal microscopy. TRAP1 staining (**m**), MitoTracker (**n**, **o**) and DAPI (**o**) were used to visualize cellular substructures (one representative experiment shown of two independent experiments). Scale bars, 10 μm (**c**, **d**, **f**, **l**–**o**).

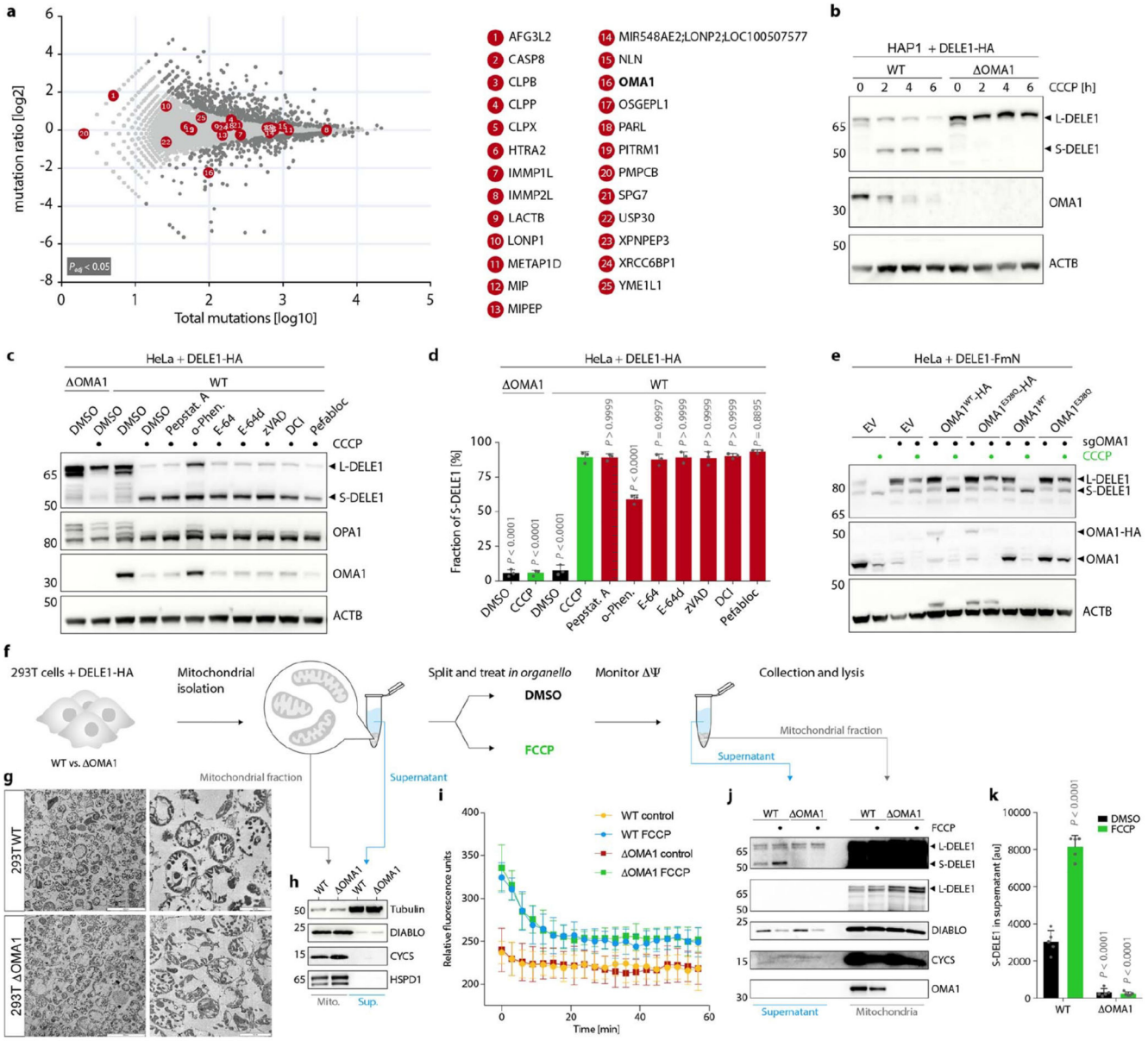

Extended Data Fig. 7. Processing of full-length DELE1 into S-DELE1 is mediated by catalytically active OMA1.

a, Data from Fig. 1a, with statistical significance of mutation enrichment assessed and visualized in the same way (two-sided Fisher's exact test, $P_{adj} < 0.05$). Known mitochondrial proteases[44,45] are highlighted in red. *XRCC6BP1* is also known as *ATP23*. **b**, Wild-type HAP1 cells and clonal OMA1 knockout cells were transfected with DELE1-HA, treated with CCCP and assayed by immunoblotting. **c**, HeLa cells of the stated genotypes were transfected with DELE1-HA and pre-treated with the indicated protease inhibitors for 5 h, followed by the addition of CCCP for 2 h. The fates of DELE1, OMA1 and OPA1 were monitored by immunoblotting. DCI, 3,4-dichloroisocoumarin; pepstat. A, pepstatin A; ophen, o-phenanthroline. **d**, Quantification of **c**. The fraction of S-DELE1 (versus L-DELE1) is indicated. Statistical significance was assessed using oneway ANOVA with

Europe PMC Funders Author Manuscripts

Tukey's multiple comparisons correction and represents the significance relative to the wild type plus CCCP condition (mean ± s.d. of $n = 3$ independent experiments). **e**, HeLa cells transiently exposed to an sgRNA directed against *OMA1* were co-transfected with the indicated cDNAs and cleavage of DELE1–Flag–mNeon (FmN) after 2 h of CCCP treatment was monitored by immunoblotting (one representative experiment shown of two independent experiments). **f**, Workflow of the in vitro assay for DELE1 fate upon mitochondrial depolarization using mitochondria purified from wild-type or OMA1-deficient 293T cells that were transiently transfected with DELE1-HA. **g**, **h**, Purity analysis of isolated mitochondria using electron microscopy (**g**) and immunoblotting (**h**) (one representative experiment shown of two independent experiments for each). For immunoblotting, around 1% of the mitochondrial and 0.2% of the cytosolic fraction was used. The electron micrographs show a high proportion and purity of mitochondria, only slight contaminations of membrane fragments or other cell organelles and the complete absence of intact cells within the mitochondrial suspensions. Scale bars, 5 μm (left) or 1 μm (right). **i**–**k**, Isolated mitochondria from **g**, **h** were treated in vitro with FCCP and analysed for DELE1 processing. **i**, Mitochondria build up a membrane potential that remains stable for one hour (demonstrated by constant low fluorescence). FCCP (500 nM) was used to induce dissipation of the mitochondrial membrane potential, yielding an increase in fluorescence. **j**, After one hour of FCCP treatment, the mitochondria and supernatant were separated by centrifugation and the protein levels in both compartments were analysed by immunoblotting (top, long exposure; bottom, short exposure for DELE1–HA) **k**, The amount of S-DELE1 in the supernatants was quantified and compared to the wild type plus DMSO condition using two-way ANOVA with Tukey's multiple comparisons correction. In **i**, **k**, data are mean ± s.d. of $n = 5$ independent experiments; **j** shows one representative experiment of $n = 5$ independent experiments, of which the purity analysis shown in **g**, **h** was performed for two independent experiments.

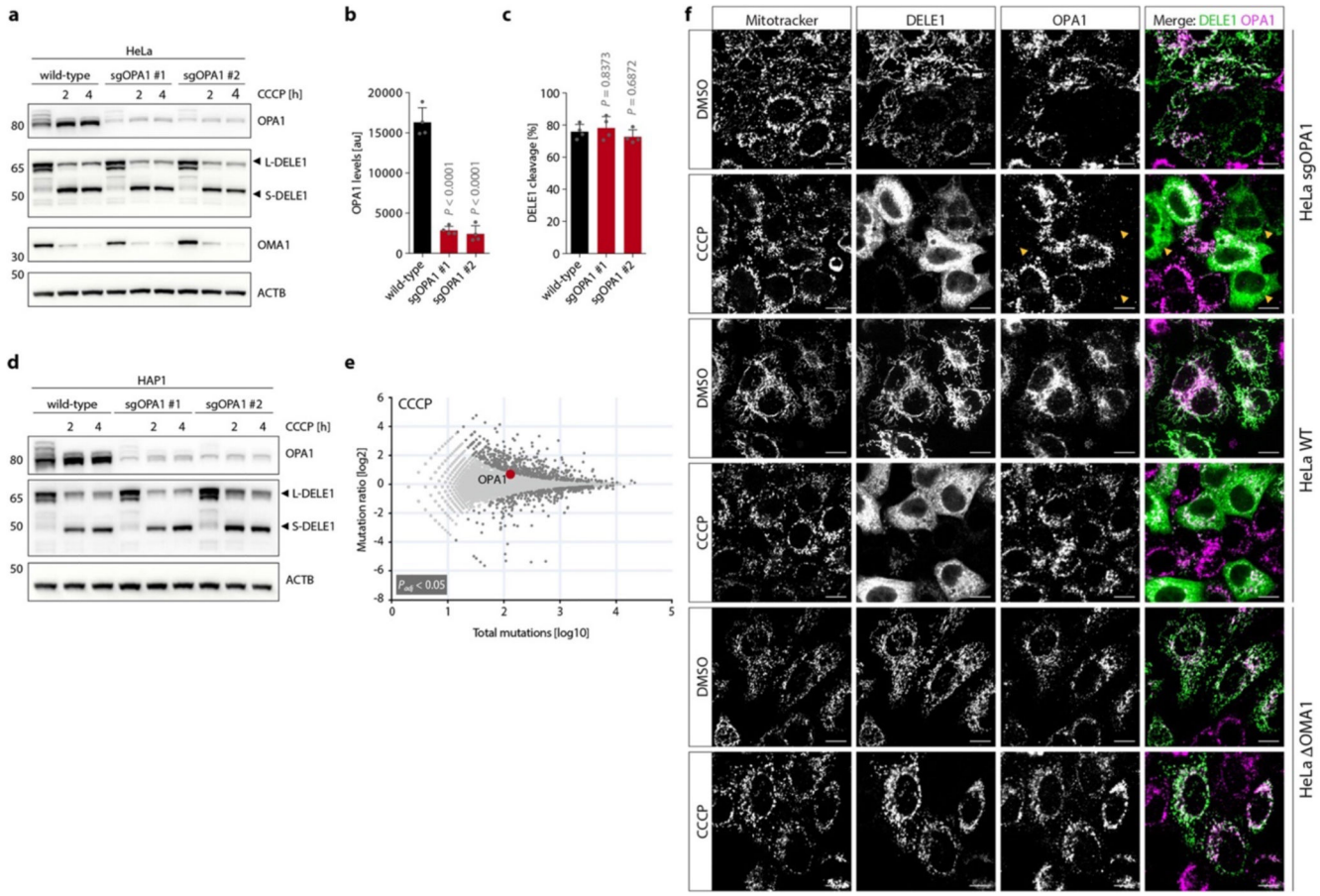

Extended Data Fig. 8. DELE1 cleavage and subcellular redistribution after CCCP treatment depend on OMA1 but not OPA1.

a–**c**, HeLa cells were treated with sgRNAs directed against *OPA1*, stimulated with CCCP and analysed as indicated together with wild-type HeLa cells by immunoblotting (**a**). OPA1 levels (**b**) and DELE1 cleavage (**c**) were quantified. Statistical significance was assessed using one-way ANOVA with Tukey's multiple comparisons correction and represents the significance relative to the wild type (mean ± s.d. of $n = 4$ biologically independent samples). **d**, HAP1 cells were treated and analysed as in **a** (one representative experiment shown of two independent experiments). **e**, Data from Fig. 1a, with statistical significance of mutation enrichment assessed and visualized in the same way (two-sided Fisher's exact test, $P_{adj} < 0.05$). OPA1 is highlighted in red. **f**, HeLa cells were treated with an sgRNA directed against *OPA1*, stimulated with CCCP and analysed for DELE1 localization and OPA1 status, alongside wild-type and OMA1-knockout cells. Arrowheads highlight OPA1-deficient cells. One representative experiment shown of two independent experiments. Scale bars, 10 μm.

Europe PMC Funders Author Manuscripts

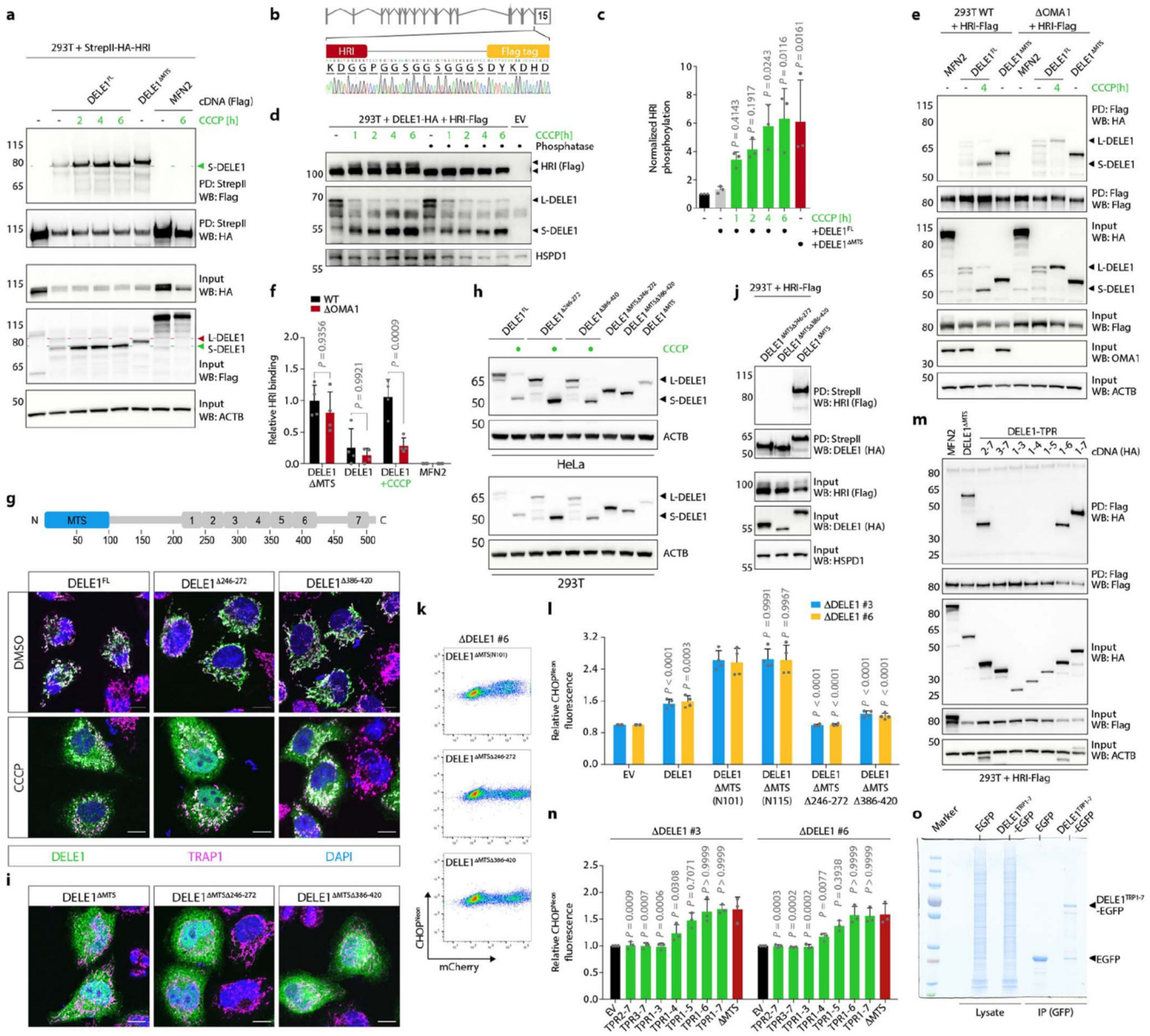

Extended Data Fig. 9. Physical interaction between DELE1 and HRI.

a, 293T cells were co-transfected with StrepTagII-HA-HRI and the indicated Flag-mNeon-tagged cDNAs before stimulation with CCCP as indicated. Cells were then lysed and StrepTagII-containing protein complexes were immobilized on Strep-Tactin beads and analysed by immunoblotting along with the input lysate. DELE1^{FL}, full-length DELE1. **b**, A C-terminal in-frame fusion of a triple Flag tag was introduced into the endogenous *EIF2AK1* (HRI) locus of 293T cells using CRISPR. **c**, Quantification of Fig. 3b. The bar chart shows the relative abundance of the slowly migrating species of HRI (phosphorylated HRI) compared to the faster migrating band. Data were normalized to the empty vector (black) and significance (compared to full-length DELE1 untreated, grey) was assessed using one-way ANOVA with Dunnett's multiple comparisons correction (mean ± s.d. of n = 3 independent experiments). **d**, 293T cells were co-transfected with HRI-Flag and DELE1-

Europe PMC Funders Author Manuscripts

HA and exposed to CCCP for the denoted amounts of time before immunoblotting. The shift in electrophoretic mobility of HRI upon activation is reversed by treatment of the lysates with alkaline phosphatase. **e**, 293T cells of the indicated genotypes were co-transfected with HRI-Flag and the specified HA-tagged constructs. After CCCP treatment, lysates were immobilized on anti-Flag beads and analysed by immunoblotting along with the input lysate (one representative experiment shown of four independent experiments). **f**, Quantification of **e**(mean ± s.d. of $n = 4$ independent experiments; two-way ANOVA with Tukey's multiple comparisons correction). **g**, HeLa cells were transiently transfected with the indicated constructs, treated with CCCP or DMSO and analysed for subcellular localization of the transfected cDNAs by HA staining and confocal microscopy with cellular structures labelled as indicated. **h**, DELE1 mutants were transiently transfected into HeLa and 293T cells before exposure to CCCP for 2 h. The processing of DELE1–HA was monitored by immunoblotting. **i**, HeLa cells were transfected as indicated and analysed for subcellular localization as in **g**. **j**, 293T cells were co-transfected with HRI-Flag and the indicated StrepTagII-HA cDNAs. Cells were then lysed and StrepTagII-containing protein complexes were immobilized on Strep-Tactin beads and analysed by immunoblotting along with the input lysate. **k**, **l**, Clonal DELE1-knockout HAP1 cells were transiently transfected with the specified cDNAs together with mCherry and induction of $CHOP^{Neon}$ was monitored by flow cytometry as in Fig. 2a. Per genotype, data were normalized to the empty vector and statistical significance (compared to DELE1(ΔMTS(N101))) was assessed using one-way ANOVA with Tukey's multiple comparisons correction (mean ± s.d. of $n = 4$ independent experiments). **m**, Wild-type 293T cells were transiently transfected with HRI-Flag and the indicated HA-tagged cDNAs and processed as in **e** (one representative experiment shown of four independent experiments). **n**, DELE1-deficient HAP1 $CHOP^{Neon}$ cells were transiently transfected as indicated and analysed by flow cytometry 32 h after transfection. Per genotype, data were normalized to the empty vector (black) and statistical significance (compared to DELE(ΔMTS)) was assessed using one-way ANOVA with Tukey's multiple comparisons correction (mean ± s.d. of $n = 3$ independent experiments). **o**, Cell lysates from Fig. 3c were analysed by Coomassie staining before (lysate) and after exposure to GFP-TRAP beads (IP (GFP)). Scale bars, 10 μm (**g**, **i**).

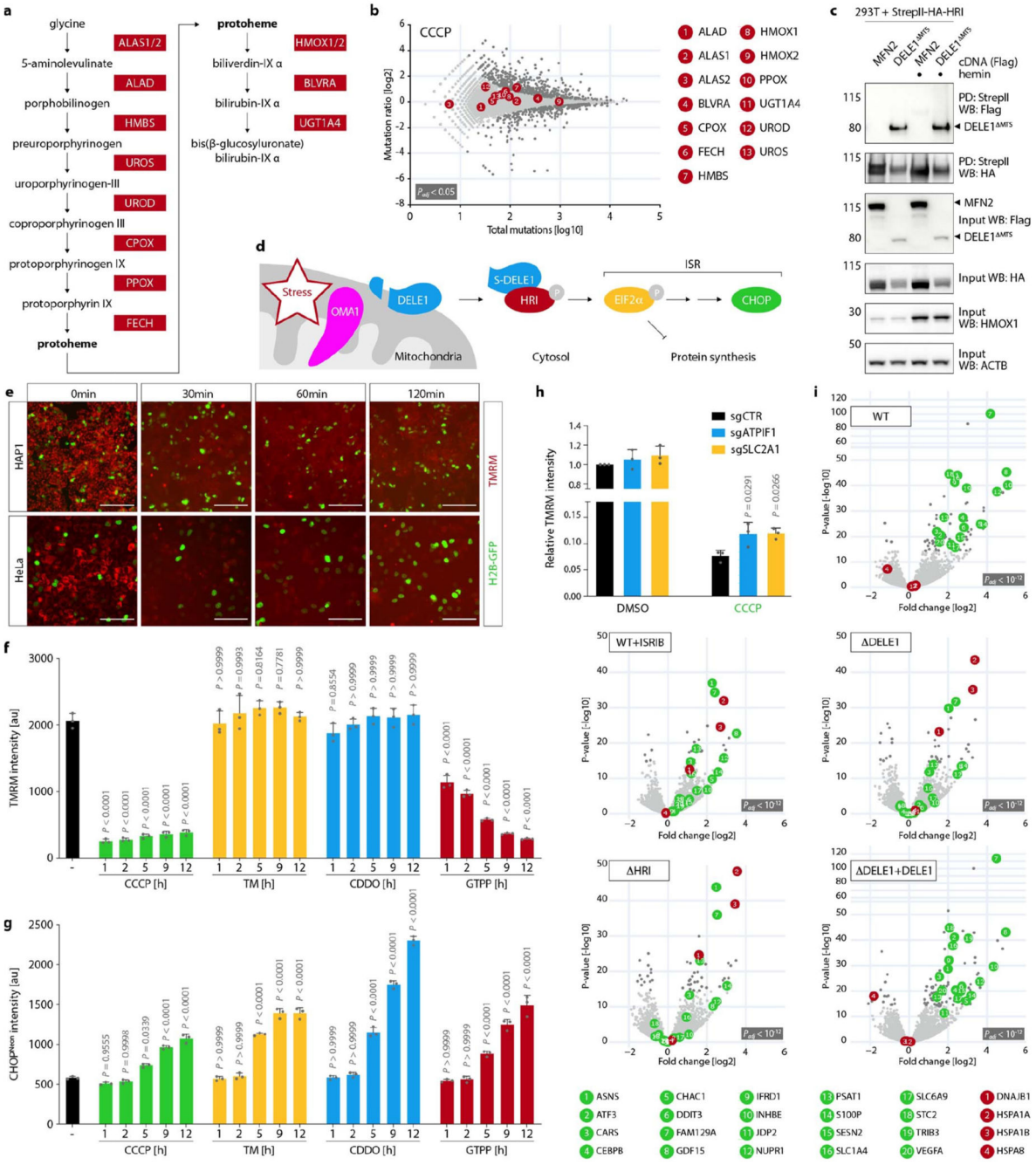

Extended Data Fig. 10. Effects of haem and mitochondrial membrane potential on the OMA1–DELE1–HRI pathway.

a, Schematic depiction of haem metabolism. **b**, Data from Fig. 1a, with statistical significance of mutation enrichment assessed and visualized in the same way (two-sided Fisher's exact test, $P_{adj} < 0.05$). Haem-related genes from **a** are highlighted in red. **c**, Immunoprecipitation experiment as in Extended Data Fig. 9a in the presence of haemin during cell culture (20 μM for 12 h before lysis) and immunoprecipitation (8 μM in lysis and wash buffers). *HMOX1* is induced in response to increased haem levels (one representative

Europe PMC Funders Author Manuscripts

experiment shown of two independent experiments). **d**, Model of the pathway identified here. Mitochondrial stress activates OMA1, which leads to cleavage of DELE1 and its subsequent cytosolic binding to and activation of HRI, triggering the ISR. **e**, Wild-type HAP1 and HeLa cells were treated with CCCP, and the mitochondrial membrane potential was visualized by TMRM using a live-cell-imaging system. H2B-GFP was transfected to stain nuclei. Scale bars, 100 μm. **f**, **g**, HAP1 $CHOP^{Neon}$ cells were stimulated as indicated, and $CHOP^{Neon}$ levels (**g**) and the mitochondrial membrane potential (**f**) were quantified by flow cytometry. Statistical significance is depicted relative to DMSO-treated control cells (mean ± s.d. of $n = 3$ independent experiments; one-way ANOVA with Tukey's multiple comparisons correction). **h**, HeLa cells were transfected with the indicated sgRNAs and the mitochondrial membrane potential was quantified after 1 h of CCCP treatment by flow cytometry. The TMRM signal was normalized to the non-targeting control sgRNA and DMSO control, and for CCCP-treated samples statistical significance was assessed relative to the non-targeting control sgRNA and CCCP (mean ± s.d. of $n = 3$ independent experiments; two-way ANOVA with Dunnett's multiple comparisons correction). **i**, Volcano plots of RNA-seq analysis of the indicated samples. For every gene, the fold change in expression after CCCP treatment (versus DMSO treatment; x axis) is plotted against the P value (two-tailed Wald test in DESeq2; y axis). Genes with a significant differential expression ($P_{adj} < 10^{-12}$ (Benjamini–Hochberg)) are depicted in dark grey. ATF4 and CHOP target genes[39,40] (green) and heat-shock proteins[43] (red) from Fig. 3e are highlighted ($n = 4$ biologically independent samples per group). *FAM129A* is also known as *NIBAN1*.

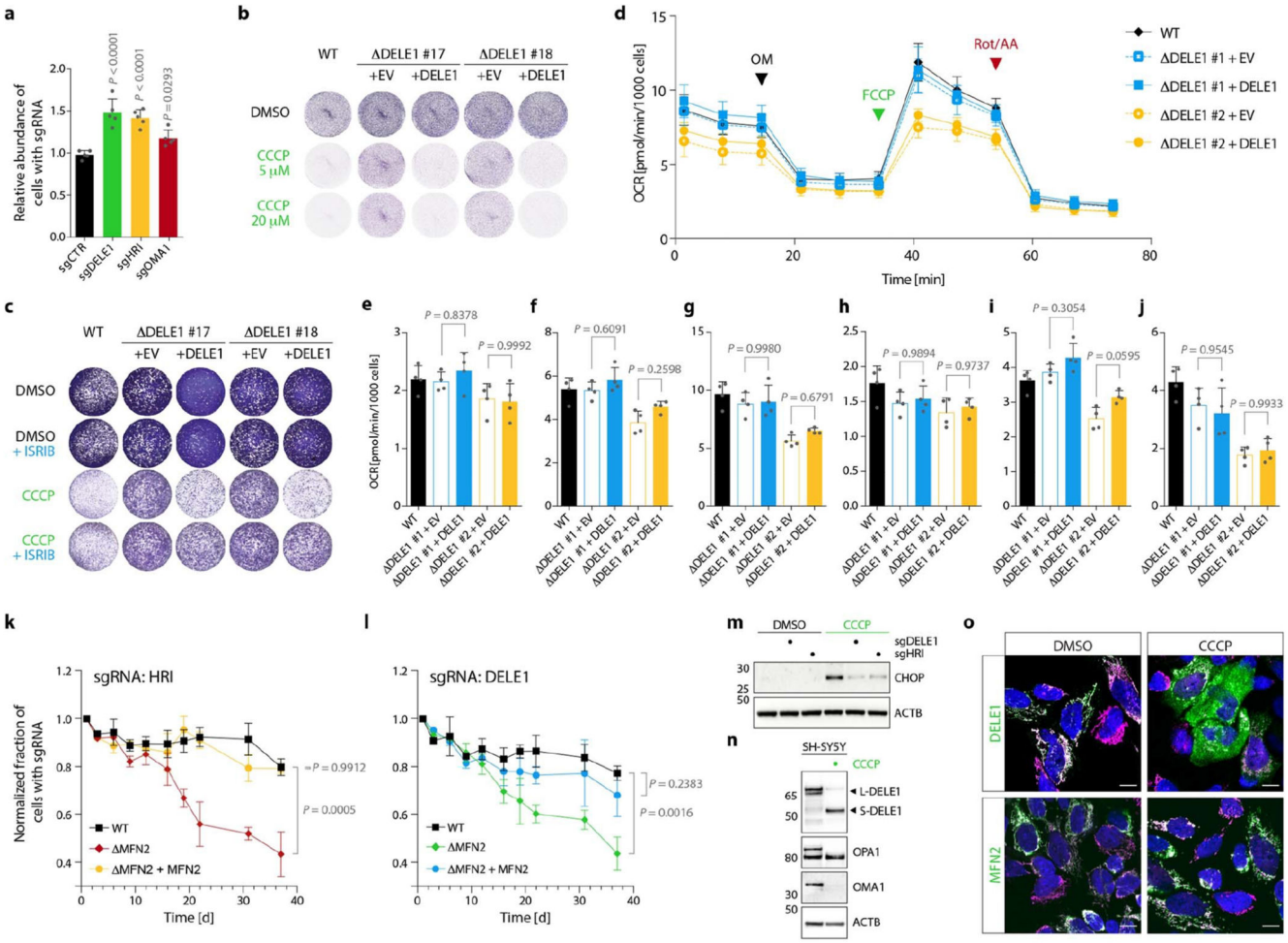

Extended Data Fig. 11. Cellular fitness and mitochondrial function in cells in which the DELE1–HRI–eIF2α axis is perturbed.

a, HAP1 cells were infected with lentivirus expressing TagRFP and the indicated sgRNAs. A 1:1 mixture of infected and uninfected cells was treated for 48 h with 5 μM CCCP or DMSO and analysed by flow cytometry. The abundance of RFP^+ sgRNA-containing cells after CCCP treatment was compared with the respective DMSO-treated sample bearing the same sgRNA and normalized to a non-targeting control sgRNA. Statistical significance was assessed compared to a second non-targeting control sgRNA using one-way ANOVA with Dunnett's multiple comparisons correction (mean ± s.d. of $n = 5$ independent experiments). **b**, **c**, HAP1 cells of the indicated genotypes were treated as indicated for 48 h and cell survival was visualized using crystal violet (one representative experiment shown of three independent experiments). **d**–**j**, Wild-type and DELE1-knockout HeLa cells stably expressing the indicated cDNAs were subjected to different mitochondrial stressors and the oxygen consumption rate (OCR) was monitored. Within the same clonal background, no significant difference between DELE1-deficient and DELE1-proficient cells could be observed in non-mitochondrial oxygen consumption (**e**), basal respiration (**f**), maximal respiration (**g**), proton leak (**h**), ATP production (**i**) and spare respiratory capacity (**j**). Mean ± s.d. of $n = 4$ independent culture wells from one representative experiment of three

Europe PMC Funders Author Manuscripts

independent experiments is shown; statistical significance was assessed using one-way ANOVA with Tukey's multiple comparisons correction. **k**, **l**, Wild-type, MFN2-knockout and stably reconstituted HAP1 cells were lentivirally transduced with a construct encoding TagRFP together with a non-targeting control sgRNA or an sgRNA directed against *EIF2AK1* (HRI) (**k**) or *DELE1* (**l**) and the fraction of RFP^+ cells was monitored over time. The abundance of sgDELE1 or sgHRI-containing cells was normalized to non-targeting sgRNA and to time 0 (mean ± s.d. of $n = 3$ biologically independent, separately infected and cultured wells per sgRNA and genotype; one-way ANOVA with Dunnett's multiple comparisons correction; one representative experiment shown of two independent experiments). **m**, SH-SY5Y cells were exposed to the indicated sgRNAs and treated as in Extended Data Fig. 5c (one representative experiment shown of four independent experiments). **n**, **o**, Processing and cellular localization of DELE1–HA in SH-SY5Y cells, as in Extended Data Fig. 6k, o. MFN2–Flag–mNeon served as a control (one representative experiment shown of two independent experiments). Scale bars, 10 μm.

Supplementary Material

Refer to Web version on PubMed Central for supplementary material.

Acknowledgements

We thank A. Graf and H. Blum for deep-sequencing infrastructure; C. Jung for assistance with confocal microscopy; N. Tafrishi for assistance with cell sorting; S. Theurich for access to Seahorse instrumentation; T. Brummelkamp and V. Hornung for valuable comments on the manuscript; and J. Stingele, R. Beckmann and all members of the Jae lab for helpful discussions. This work was supported by ERC StG 804182 (SOLID), the Center for Integrated Protein Science Munich and the German Research Foundation (Heinz-Maier-Leibnitz Prize) to L.T.J.

References

1. Higuchi-Sanabria R, Frankino PA, Paul JW III, Tronnes SU, Dillin A. A futile battle? Protein quality control and the stress of aging. Dev Cell. 2018; 44:139–163. [PubMed: 29401418]
2. Shpilka T, Haynes CM. The mitochondrial UPR: mechanisms, physiological functions and implications in ageing. Nat Rev Mol Cell Biol. 2018; 19:109–120. [PubMed: 29165426]
3. Sun N, Youle RJ, Finkel T. The mitochondrial basis of aging. Mol Cell. 2016; 61:654–666. [PubMed: 26942670]
4. Quirós PM, et al. Multi-omics analysis identifies ATF4 as a key regulator of the mitochondrial stress response in mammals. J Cell Biol. 2017; 216:2027–2045. [PubMed: 28566324]
5. Harding HP, et al. An integrated stress response regulates amino acid metabolism and resistance to oxidative stress. Mol Cell. 2003; 11:619–633. [PubMed: 12667446]
6. Taniuchi S, Miyake M, Tsugawa K, Oyadomari M, Oyadomari S. Integrated stress response of vertebrates is regulated by four eIF2α kinases. Sci Rep. 2016; 6:32886. [PubMed: 27633668]
7. Münch C, Harper JW. Mitochondrial unfolded protein response controls matrix pre-RNA processing and translation. Nature. 2016; 534:710–713. [PubMed: 27350246]
8. Palam LR, Baird TD, Wek RC. Phosphorylation of eIF2 facilitates ribosomal bypass of an inhibitory upstream ORF to enhance CHOP translation. J Biol Chem. 2011; 286:10939–10949. [PubMed: 21285359]
9. Brockmann M, et al. Genetic wiring maps of single-cell protein states reveal an off-switch for GPCR signalling. Nature. 2017; 546:307–311. [PubMed: 28562590]
10. Azim M, Surani H. Glycoprotein synthesis and inhibition of glycosylation by tunicamycin in preimplantation mouse embryos: compaction and trophoblast adhesion. Cell. 1979; 18:217–227. [PubMed: 509524]

11. Yore MM, Kettenbach AN, Sporn MB, Gerber SA, Liby KT. Proteomic analysis shows synthetic oleanane triterpenoid binds to mTOR. PLoS One. 2011; 6:e22862. [PubMed: 21818401]
12. Harada T, Iwai A, Miyazaki T. Identification of DELE, a novel DAP3-binding protein which is crucial for death receptor-mediated apoptosis induction. Apoptosis. 2010; 15:1247–1255. [PubMed: 20563667]
13. Tanaka A, et al. Proteasome and p97 mediate mitophagy and degradation of mitofusins induced by Parkin. J Cell Biol. 2010; 191:1367–1380. [PubMed: 21173115]
14. Baker MJ, et al. Stress-induced OMA1 activation and autocatalytic turnover regulate OPA1-dependent mitochondrial dynamics. EMBO J. 2014; 33:578–593. [PubMed: 24550258]
15. Sekine S, et al. Reciprocal roles of Tom7 and OMA1 during mitochondrial import and activation of PINK1. Mol Cell. 2019; 73:1028–1043. [PubMed: 30733118]
16. Scheufler C, et al. Structure of TPR domain–peptide complexes: critical elements in the assembly of the Hsp70–Hsp90 multichaperone machine. Cell. 2000; 101:199–210. [PubMed: 10786835]
17. Lu L, Han AP, Chen J-J. Translation initiation control by heme-regulated eukaryotic initiation factor 2α kinase in erythroid cells under cytoplasmic stresses. Mol Cell Biol. 2001; 21:7971–7980. [PubMed: 11689689]
18. Shah DI, et al. Mitochondrial Atpif1 regulates haem synthesis in developing erythroblasts. Nature. 2012; 491:608–612. [PubMed: 23135403]
19. Sukumar M, et al. Mitochondrial membrane potential identifies cells with enhanced stemness for cellular therapy. Cell Metab. 2016; 23:63–76. [PubMed: 26674251]
20. Baricault L, et al. OPA1 cleavage depends on decreased mitochondrial ATP level and bivalent metals. Exp Cell Res. 2007; 313:3800–3808. [PubMed: 17826766]
21. Sorrentino V, et al. Enhancing mitochondrial proteostasis reduces amyloid-β proteotoxicity. Nature. 2017; 552:187–193. [PubMed: 29211722]
22. Sidrauski C, et al. Pharmacological brake-release of mRNA translation enhances cognitive memory. eLife. 2013; 2:e00498. [PubMed: 23741617]
23. Züchner S, et al. Mutations in the mitochondrial GTPase mitofusin 2 cause Charcot–Marie–Tooth neuropathy type 2A. Nat Genet. 2004; 36:449–451. [PubMed: 15064763]
24. Dickson MA, et al. Human keratinocytes that express hTERT and also bypass a $p16^{INK4a}$-enforced mechanism that limits life span become immortal yet retain normal growth and differentiation characteristics. Mol Cell Biol. 2000; 20:1436–1447. [PubMed: 10648628]
25. Schmid-Burgk JL, Höning K, Ebert TS, Hornung V. CRISPaint allows modular base-specific gene tagging using a ligase-4-dependent mechanism. Nat Commun. 2016; 7:12338. [PubMed: 27465542]
26. Jae LT, et al. Lassa virus entry requires a trigger-induced receptor switch. Science. 2014; 344:1506–1510. [PubMed: 24970085]
27. Carette JE, et al. Haploid genetic screens in human cells identify host factors used by pathogens. Science. 2009; 326:1231–1235. [PubMed: 19965467]
28. Langmead B, Trapnell C, Pop M, Salzberg SL. Ultrafast and memory-efficient alignment of short DNA sequences to the human genome. Genome Biol. 2009; 10:R25. [PubMed: 19261174]
29. Quinlan AR, Hall IM. BEDTools: a flexible suite of utilities for comparing genomic features. Bioinformatics. 2010; 26:841–842. [PubMed: 20110278]
30. Schindelin J, et al. Fiji: an open-source platform for biological-image analysis. Nat Methods. 2012; 9:676–682. [PubMed: 22743772]
31. Schmitt S, et al. A semi-automated method for isolating functionally intact mitochondria from cultured cells and tissue biopsies. Anal Biochem. 2013; 443:66–74. [PubMed: 23969012]
32. Bradford MM. A rapid and sensitive method for the quantitation of microgram quantities of protein utilizing the principle of protein-dye binding. Anal Biochem. 1976; 72:248–254. [PubMed: 942051]
33. Zamzami N, Métivier D, Kroemer G. Quantitation of mitochondrial transmembrane potential in cells and in isolated mitochondria. Methods Enzymol. 2000; 322:208–213. [PubMed: 10914018]
34. Zischka H, et al. Electrophoretic analysis of the mitochondrial outer membrane rupture induced by permeability transition. Anal Chem. 2008; 80:5051–5058. [PubMed: 18510346]

35. Afgan E, et al. The Galaxy platform for accessible, reproducible and collaborative biomedical analyses: 2018 update. Nucleic Acids Res. 2018; 46:W537–W544. [PubMed: 29790989]
36. Love MI, Huber W, Anders S. Moderated estimation of fold change and dispersion for RNA-seq data with DESeq2. Genome Biol. 2014; 15:550. [PubMed: 25516281]
37. de Hoon MJL, Imoto S, Nolan J, Miyano S. Open source clustering software. Bioinformatics. 2004; 20:1453–1454. [PubMed: 14871861]
38. Saldanha AJ. Java Treeview—extensible visualization of microarray data. Bioinformatics. 2004; 20:3246–3248. [PubMed: 15180930]
39. Han H, et al. TRRUST v2: an expanded reference database of human and mouse transcriptional regulatory interactions. Nucleic Acids Res. 2018; 46:D380–D386. [PubMed: 29087512]
40. Bao XR, et al. Mitochondrial dysfunction remodels one-carbon metabolism in human cells. eLife. 2016; 5:e10575. [PubMed: 27307216]
41. Ashburner M, et al. Gene ontology: tool for the unification of biology. Nat Genet. 2000; 25:25–29. [PubMed: 10802651]
42. The Gene Ontology Consortium. The Gene Ontology resource: 20 years and still GOing strong. Nucleic Acids Res. 2019; 47:D330–D338. [PubMed: 30395331]
43. Carbon S, et al. AmiGO: online access to ontology and annotation data. Bioinformatics. 2009; 25:288–289. [PubMed: 19033274]
44. Quirós PM, Langer T, López-Otín C. New roles for mitochondrial proteases in health, ageing and disease. Nat Rev Mol Cell Biol. 2015; 16:345–359. [PubMed: 25970558]
45. Calvo SE, Clauser KR, Mootha VK. MitoCarta2.0: an updated inventory of mammalian mitochondrial proteins. Nucleic Acids Res. 2016; 44:D1251–D1257. [PubMed: 26450961]

Europe PMC Funders Author Manuscripts

Europe PMC Funders Author Manuscripts

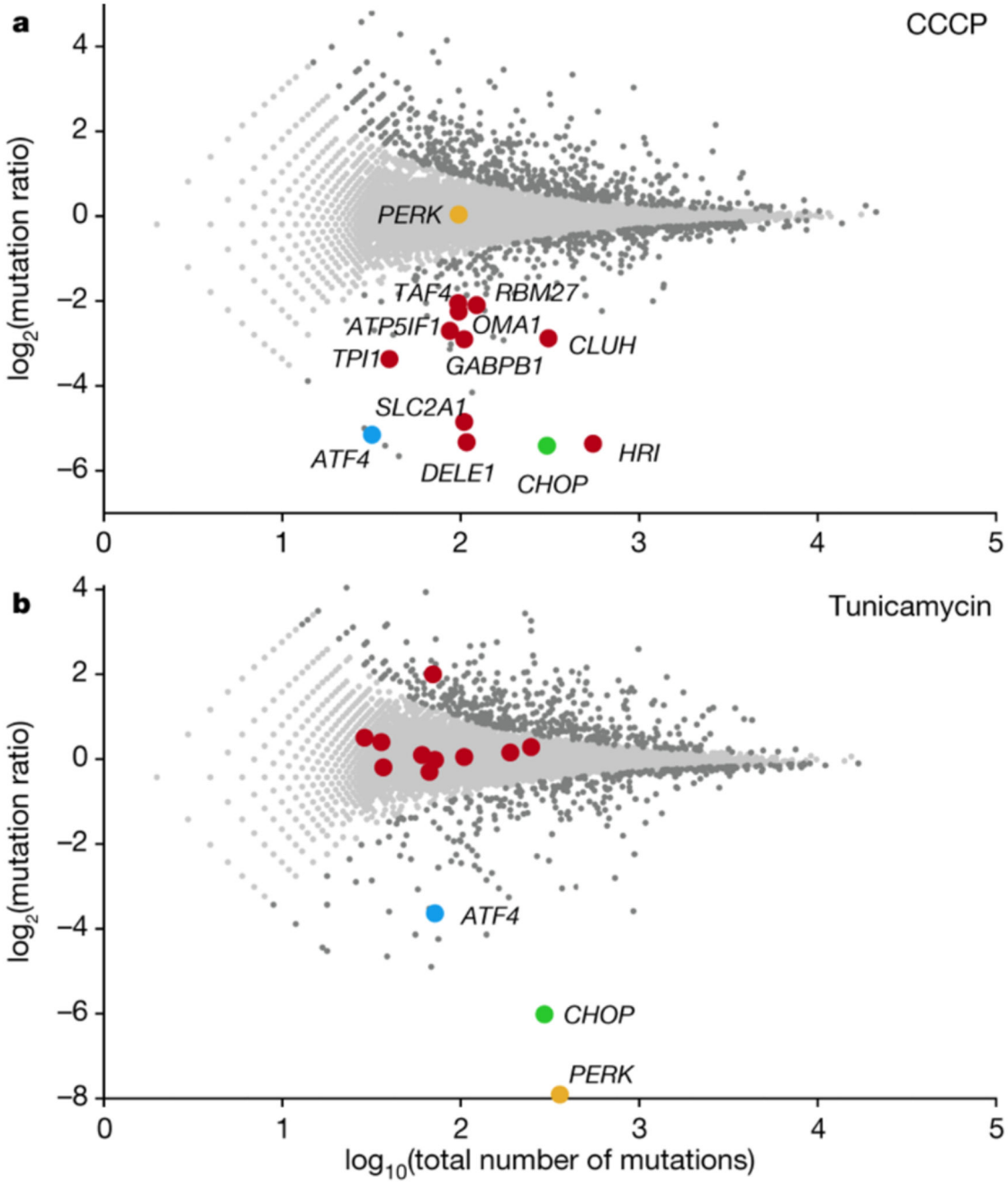

Fig. 1. Genome-wide perturbation profiling reveals regulators of CHOP in the context of different triggers of the ISR.

a, **b**, Genetic screens showing positive and negative regulators of CHOP^{Neon} in cells that were treated with CCCP (**a**) or tunicamycin (**b**). Per gene (dots), the ratio of the mutation frequency in cells with high CHOP^{Neon} expression versus cells with low CHOP^{Neon} expression (*y* axis) is plotted against the combined number of unique mutations identified in both populations of cells (*x* axis) ($n = 2.12 \times 10^7$ (**a**) or 2.07×10^7 (**b**) interrogated single cells). Genes enriched for mutations are shown in dark grey (two-sided Fisher's exact test,

false discovery rate (FDR)-corrected *P* value (P_{adj}) < 0.05). Red dots specify genes that are highly significant in the CCCP dataset but not in the tunicamycin or CDDO datasets. *PERK* is also known as *EIF2AK3*.

Europe PMC Funders Author Manuscripts

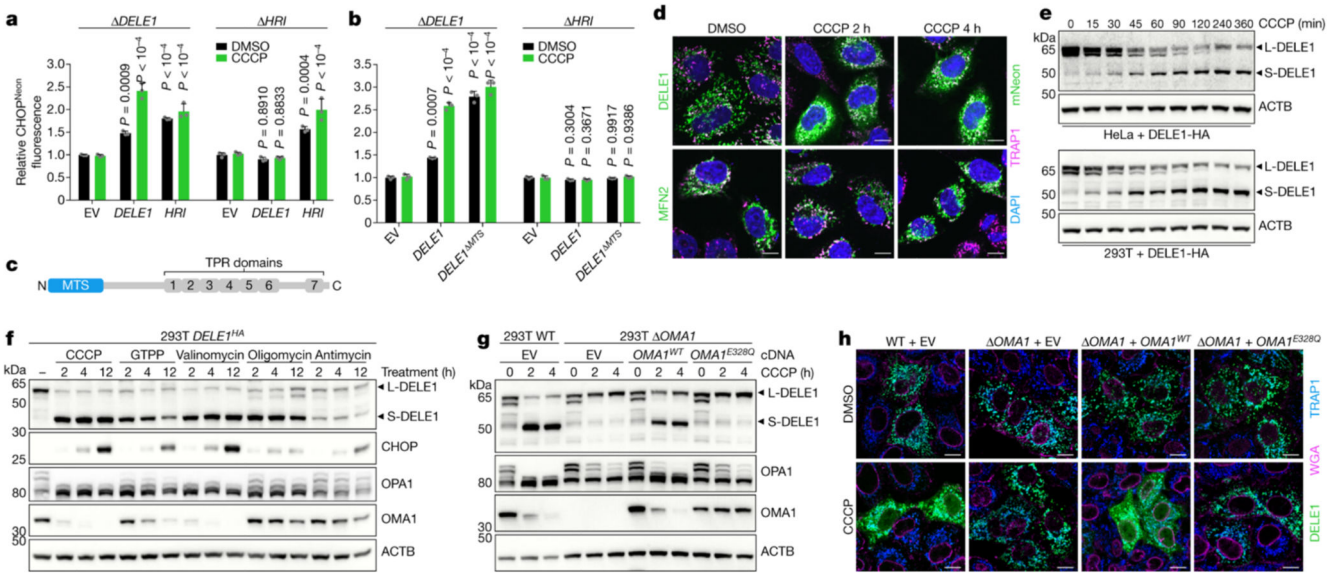

Fig. 2. DELE1 operates upstream of HRI and accumulates in the cytosol after OMA1-mediated cleavage.

a, **b**, HAP1 CHOP^{Neon} cells of the specified genotypes (Δ*DELE1* or Δ*HRI*), transiently transfected with the indicated cDNAs or empty vector (EV), were treated for 9 h with CCCP or DMSO control and analysed by flow cytometry. The CHOP^{Neon} fluorescence intensity for each genotype was normalized to the empty vector plus DMSO condition, and compared with the empty vector for each treatment (mean ± s.d. of $n = 3$ independent biological samples; two-way ANOVA with Tukey's multiple comparisons correction; one representative experiment shown of six independent experiments). **c**, Domain architecture of DELE1. **d**, Confocal microscopy of DELE1–Flag–mNeon and MFN2–Flag–mNeon expressed in HeLa cells. **e**, HeLa cells (top) or 293T cells (bottom) transfected with haemagglutinin (HA)-tagged DELE1 (DELE1-HA) were treated with CCCP for the indicated time periods before analysis of DELE1 cleavage by HA immunoblotting. L-DELE1 indicates the longer version of DELE1. **f**, Cells expressing endogenous HA-tagged DELE1 (*DELE1*^{HA}) were stimulated as indicated and analysed by immunoblotting. **g**, Wild-type (WT) and clonal OMA1-knockout (Δ*OMA1*) cells, reconstituted with the specified cDNAs, were transfected with DELE1-HA, treated with CCCP for the indicated periods and assayed by immunoblotting. **h**, Wild-type and clonal OMA1-knockout HeLa cells were transfected with the indicated cDNAs, treated with CCCP or DMSO control and assayed by confocal microscopy. DAPI (**d**) and wheat-germ agglutinin (WGA; **h**) staining identify the nuclei and cell membranes, respectively; TRAP1 staining identifies mitochondria. Scale bars, 10 μm (**d**, **h**).

Europe PMC Funders Author Manuscripts

Europe PMC Funders Author Manuscripts

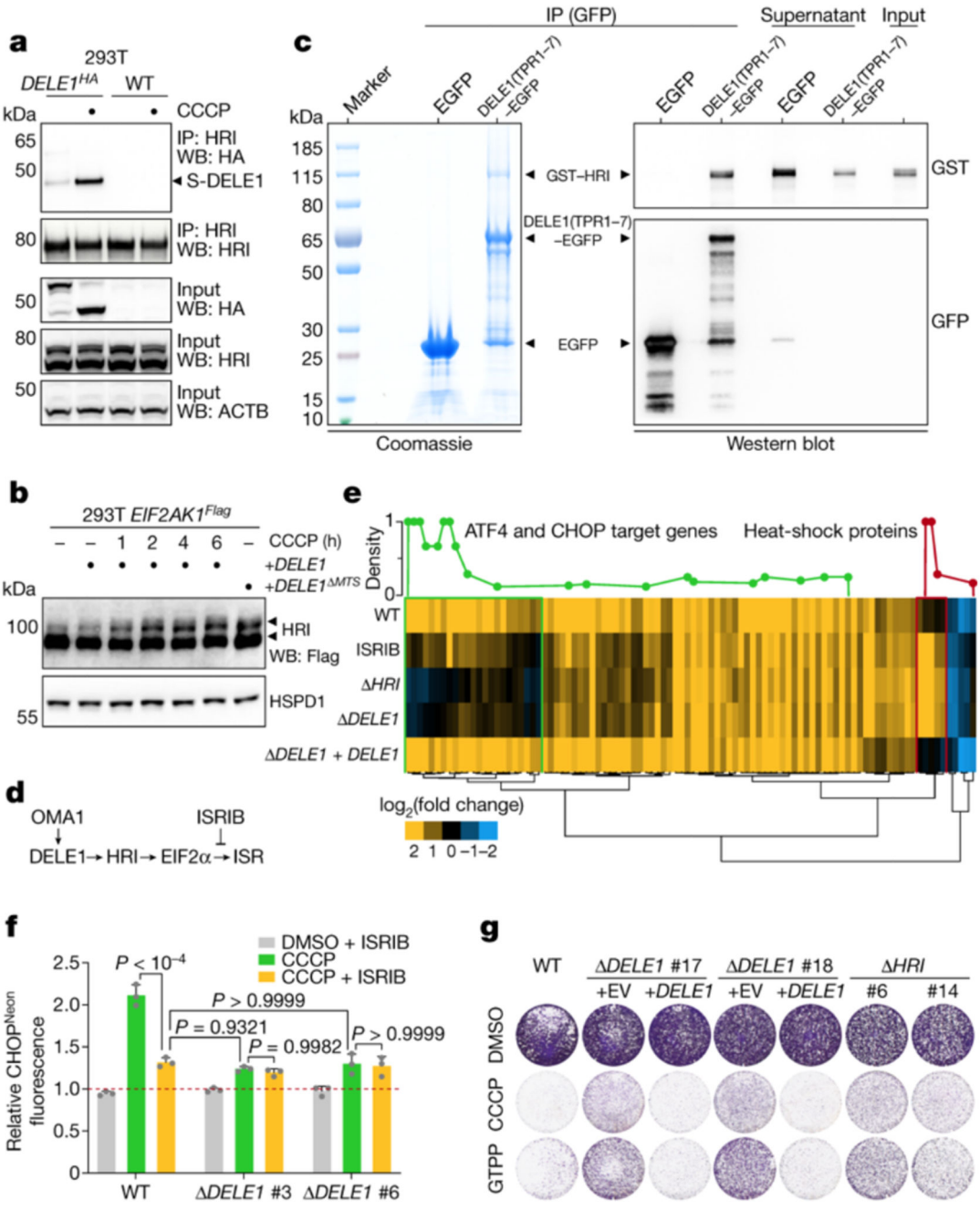

Fig. 3. DELE1 binds to HRI in the cytosol, and a deficiency in this pathway mimics ISR inhibition and alters fitness in the context of mitochondrial stress.

a, Endogenous HRI was immobilized on beads and its ability to co-precipitate endogenous HA-tagged DELE1 (*DELE1*^{HA}) was analysed by immunoblotting. IP, immunoprecipitation; WB, western blot. **b**, Shift in electrophoretic mobility of endogenous Flag-tagged HRI (*EIF2AK1*^{Flag}) after the indicated treatments. **c**, EGFP or DELE1(TRP1–7)–EGFP were stringently purified from 293T cells that were treated with an sgRNA to deplete HRI and incubated with glutathione *S*-transferase (GST)-tagged HRI produced in *E. coli*. Interaction

was assessed by Coomassie staining and immunoblotting. GST–HRI co-precipitation is accompanied by its depletion from the corresponding supernatant. **d**, Model of the pathway. **e**, Transcriptomic profiling of wild-type HAP1 cells (with or without ISRIB treatment) and knockout mutants after treatment with CCCP for 12 h ($n = 4$ independent biological samples per group). Differentially expressed genes after CCCP treatment (two-tailed Wald test in DESeq2, $P_{adj} < 10^{-12}$, $|\log_2$-transformed fold change$| > 1.5$) were hierarchically clustered. ATF4 and CHOP target genes are enriched among genes that are strongly induced in cells proficient in DELE1–HRI–eIF2α signalling but not in cells deficient in this pathway (two-sided Fisher's exact test, $P_{adj} < 2 \times 10^{-19}$, green box); heat-shock proteins are enriched in the cluster of genes induced in the opposite samples ($P_{adj} < 3 \times 10^{-7}$, red box). **f**, HAP1 $CHOP^{Neon}$ cells of the specified genotypes (wild-type and DELE1-deficient clones #3 and #6) were treated as indicated for 9 h and analysed by flow cytometry. The $CHOP^{Neon}$ fluorescence intensity for each genotype was normalized to its DMSO control (red dotted line; mean ± s.d. of $n = 3$ independent experiments; two-way ANOVA with Tukey's multiple comparisons correction). **g**, HAP1 cells of the specified genotypes were treated as indicated for 48 h and surviving cells were stained with crystal violet ($n = 2$ independent experiments).